An investigation of a Devonian/Carboniferous Boundary section on the Bolivian Altiplano

Jon A. Lakin ⓘ, John E.A. Marshall and Ian Troth

Ocean and Earth Science, University of Southampton, National Oceanography Centre, European Way, Southampton SO14 3ZH, UK

CAMBRIDGE
UNIVERSITY PRESS

Abstract

The Devonian/Carboniferous Boundary (DCB) interval is associated with mass extinction, isotope excursions and a short glacial episode. This study investigates how boundary extinction and environmental change is expressed in the glacial high-palaeolatitudinal record of the Bolivian Altiplano (western Gondwana). A latest Devonian and early Carboniferous section has been investigated using sedimentology, palynology, total organic carbon and bulk $\delta^{13}C_{organic}$. The Colpacucho Formation is a Late Devonian shelfal–marine siliciclastic sequence. It is overlain in the study area by a unit of coarse sandstones and sandy diamictites, interpreted as glaciomarine. This distinctive glaciomarine unit is at least 7 km wide and 60–120 m thick with a variably incisive basal contact (<100 m). It is of very latest Famennian age and is a stratigraphic equivalent of proven glacigenic deposits across central South America. The offshore marine Kasa Formation overlies the glacigenic unit above a basal flooding surface. The DCB is 12 m above this flooding surface on the last occurrence of *Retispora lepidophyta* and significant palynological assemblage changes. This includes the loss of the *Umbellasphaeridium saharicum* phytoplankton bioprovince, endemic to Gondwana. Marine and terrestrial palynological extinctions are synchronous with a 2 ‰ positive carbon isotope excursion interpreted to be reflective of changes in organic matter delivery and preservation during an interval of environmental stress. These results inform wider debates on global environmental change and mass extinction at the DCB.

1. Introduction

End Devonian Mass Extinction (EDME) was a severe and distinct biotic crisis affecting terrestrial and marine ecosystems in the latest Famennian Stage (Fig. 1). It was coincident with a short glacial episode within the range of *Retispora lepidophyta* – a cosmopolitan miospore of latest Famennian age (Maziane *et al.* 1999; Caputo *et al.* 2008; Isaacson *et al.* 2008; Lakin *et al.* 2016). Proven glacigenic deposits are described in central South America (Díaz-Martínez & Isaacson, 1994; Cunha *et al.* 2007; Vaz et al. 2007; Wicander *et al.* 2011; Caputo & Dos Santos, 2019) and the Appalachian Basin of North America (Brezinski *et al.* 2008, 2010). These indicate a near-polar ice centre in western Gondwana and a temperate ice centre in the southern margin of Euramerica respectively (Fig. 2).

EDME is also known as the Hangenberg Crisis in the Rhenish Massif standard succession. It was of 100–300 ka duration and has been divided into three main intervals (Kaiser *et al.* 2016). The lower crisis interval (or Hangenberg Black Shale event – HBS) is associated with high-total-organic-carbon (TOC) black shales, positive carbon isotope excursions (PCIEs), and widespread marine anoxia, e.g. in Europe (Brand *et al.* 2004; Buggisch & Joachimski, 2006; Kaiser *et al.* 2013; Kumpan *et al.* 2013, 2014), China (Qie *et al.* 2015), Vietnam (Komatsu *et al.* 2014), Tibet (Liu *et al.* 2019) and North America (Saltzman, 2005; Cramer *et al.* 2008; Myrow *et al.* 2011, 2013; Over, 2020). The HBS is commonly interpreted as transgression, but it also contains regressive proxies and so could more likely represent increased terrigenous input onto carbonate shelves (Kaiser *et al.* 2011; Bábek *et al.* 2016). Extinction primarily affected marine organisms, such as ammonoids, trilobites and conodonts (Becker, 1992; Chlupac *et al.* 2000; Corradini *et al.* 2013; Kaiser *et al.* 2016). Recent reinvestigations of European and Vietnamese sections show a more complicated picture. Firstly, anoxic conditions sometimes persist into the lower Tournaisian (Paschall *et al.* 2019). And secondly, corresponding negative carbon isotope excursions (NCIEs) are recognized preceding the HBS in the upper *praesulcata* zone / lower *costatus–kockeli* interregnum zone and Devonian/Carboniferous Boundary (DCB) (Matyja *et al.* 2020; Pisarzowska & Racki, 2020; Pisarzowska *et al.* 2020).

The middle crisis interval is characterized by eustatic sea-level fall and deposition of the 'Hangenberg Sandstone' and equivalents (van Steenwinkel, 1993). Eustatic sea-level fall immediately below the DCB is supported by regressive facies and/or detrital indicators observed from diverse geological settings (see Kaiser *et al.* 2008; Weber et al. 2008; Kumpan *et al.* 2013, 2014; Bábek *et al.* 2016; Carmichael *et al.* 2016). Kaiser *et al.* (2011) estimated *c.* 100 m of relative

Age (Ma)	Period	Stage	Miospore (W. Eur.)	Miospore (S. Am.)	Conodont zonation	Miospore occurrences	Events	Rhenish standard succession	Glaciation
348	Carboniferous (Mississippian)	Tournaisian	Pu	✕	*Scalliognathus anchoralis - Doliognatus latus*			Schwarze Kieselschiefer	
350			CM						
			PC	PD	upper *Gnathodus typicus*	*C. decorus*			
352			BP	BL	*Siphonodella isostichia - S. crenulata*	*S. balteatus* / *N. loganensis*		Alum Shale	
354			HD	AL					
356					*Siphonodella crenulata*	*W. lanzonii*	Lower Alum Shale event	Hangenberg Limestone	
358			VI	✕	*Siphonodella sandbergi*				
					Siphonodella jii				
					Siphonodella duplicata				
					Siphonodella bransoni				
					Siphonodella sulcata / Protognathodus kuehni				
360	Devonian	Famennian	LN	LVa	*Protognathodus kockeli* costatus - kockeli Interregnum (CKI)	*R. lepidophyta* / *V. nitidus*	Upper crisis int.	Stockum Lst	
			LE	Rle	*Siphonodella praesulcata*	*V. vallatus* / *I. explanatus*	Mid. crisis int. / Lower crisis interval	HSh / HSst / HBS / DS	
			LL	✕	*Bispathodus ultimus ultimus*	*R. lepidophyta* / *K. literatus*	EDME	Wocklum Limestone	

Fig. 1. Chronostratigraphy of the latest Famennian (Devonian) and Tournaisian (Mississippian) Stages. Standard conodont schemes from Aretz *et al.* (2016) and Becker *et al.* (2020). Standard Western European miospore biostratigraphic schemes and occurrences from Streel *et al.* (1987) and Maziane *et al.* (1999). Those from South America are from Melo & Playford (2012) and Playford & Melo (2012) with gaps in the type sections indicated by crosses. EDME crisis intervals are from Becker *et al.* (2016). Rhenish Massif Standard Succession from Becker *et al.* (2016) and Herbig *et al.* (2019). DS = Drewer Sandstone, HBS = Hangenberg Black Shale, HSh = Hangenberg Shale, HSst = Hangenberg Sandstone, Lst = Limestone. Proven glacial deposits are found within the range of *R. lepidophyta*, mostly LE/LN, and the mid-Tournaisian PC/PD zones (see Lakin *et al.* 2016).

Fig. 2. Early Mississippian (350 Ma) palaeogeography, redrawn from Domeier & Torsvik (2014). 'S. Am' and 'N. Am' are South America and North America, respectively. Latest Famennian ice centres are highlighted. Proven glacigenic deposits are found in: (1) Brazil (Cunha *et al.* 2007; Filho *et al.* 2007; Milani *et al.*, 2007; Vaz *et al.* 2007; Caputo *et al.* 2008; Melo & Playford, 2012); (2) Bolivia (Díaz-Martínez & Isaacson, 1994; Isaacson *et al.*, 1995; Wicander *et al.* 2011); and (3) Appalachia (Ettensohn *et al.*, 2009; Brezinski *et al.* 2010). Putative ice centres are documented in (4) Africa by Theron (1993), Evans (1999), Streel & Theron (1999), Klett (2000), Streel *et al.* (2000), Almond *et al.* (2002) and Isaacson *et al.* (2008).
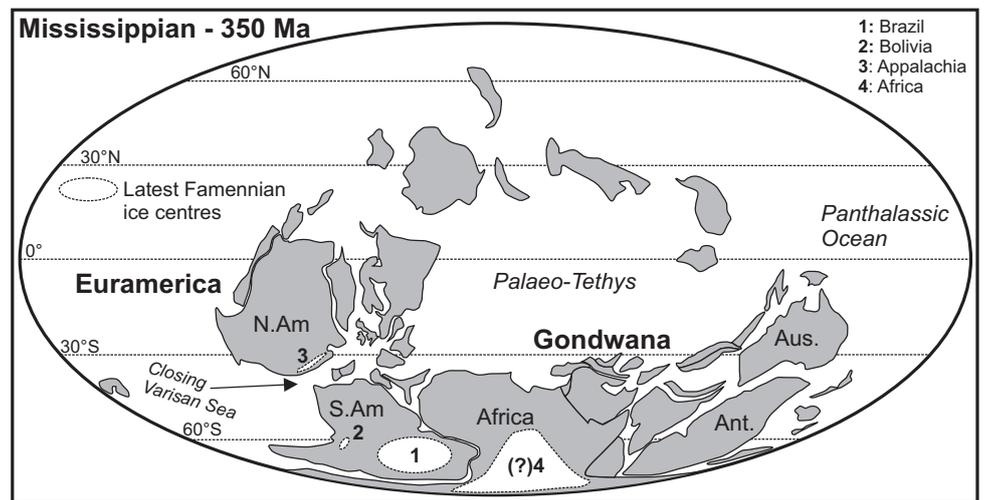
sea-level fall in Morocco, which is comparable to the <100 m of marine incision observed in central Europe and North America (van Steenwinkel, 1993; Brezinski *et al.* 2010).

The upper crisis interval at the DCB is associated with eustatic sea-level rise and severely affected terrestrial plants/miospores, tetrapods and fish (Streel & Marshall, 2006; Sallan & Coates, 2010; Marshall, 2020).

Several factors have been proposed as causes of EDME, ranging from meteorite impacts, marine anoxia, global carbon cycle change, palaeoclimate and sea-level change, to magmatic activity (Kaiser et al. 2016; Pisarzowska *et al.* 2020).

There are relatively few studies on the nature of the DCB in the glaciated southern palaeolatitudes of western Gondwana, likely because key fossil groups are extremely rare or absent.
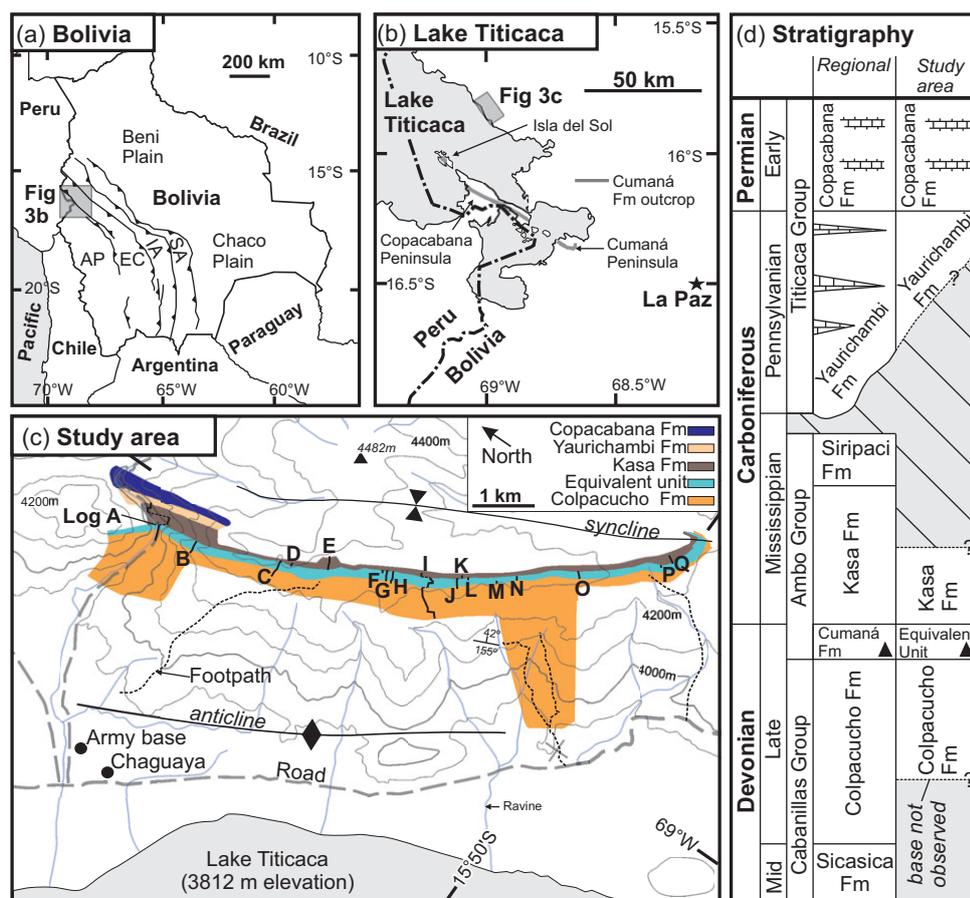
Fig. 3. (Colour online) Location maps. (a) Bolivia. (b) Lake Titicaca area. (c) Chaguaya study area with log locations and geological map overlain. (d) Bolivian Altiplano lithostratigraphy modified from Díaz-Martínez (1996) and Grader *et al.* (2007). Dark triangles in (d) indicate the units are diamictite-bearing.

Palynostratigraphy can tie Late Devonian global schemes and events into South America (e.g. Troth et al. 2011; Melo & Playford, 2012), which allows for a reinvestigation of the DCB from a siliciclastic high-palaeolatitude area affected by glaciation. Our objectives are to: (1) revisit and describe a diamictite sequence from western Gondwana (Bolivian Altiplano); (2) interpret the palynological record; and (3) test whether positive isotope excursions in organic carbon can be recognized. These results can then be compared against the global record to inform debates regarding EDME and global environmental change at the DCB.

2. Study area

The Altiplano is a high-altitude plateau formed during Andean orogenic uplift, which segmented the Palaeozoic stratigraphy into NW–SE-orientated tectonic zones (Fig. 3a; Sempere, 1995; Gregory-Wodzicki, 2000; Capitano et al., 2011; Barnes et al. 2012). Latest Famennian glacial diamictites (dropstone-in-shales) are reported in the Cumaná Formation, which crops out for c. 80 km from the Isla del Sol to the Copacabana and Cumaná Peninsulas (Fig. 3b; Díaz-Martínez & Isaacson, 1994; Díaz-Martínez et al. 1999).

The study area is on the NE shore of Lake Titicaca, near the community of Chaguaya (Fig. 3b–c). There is an uninterrupted Devonian–Mississippian sequence that contains diamictites, the global index miospore *Retispora lepidophyta* and claystones suitable for palynological recovery (Díaz-Martínez, 1992; Díaz-Martínez et al. 1999; Vavrdová & Isaacson, 1999; di Pasquo et al. 2015 di Pasquo et al. 2015 di Pasquo et al. 2015). These make it an ideal study area.

Seventeen stratigraphic logs are presented. Log A is a road section called 'Villa Molino' and Logs B–Q were measured along an approximately strike-parallel, 7 km long topographic ridgeline (Fig. 3c). The stratigraphy is mapped from field observations, log sections and satellite imagery and compared to the regional lithostratigraphy of Díaz-Martínez (1996) and Grader *et al.* (2007) (Fig. 3c–d). The Cumaná and Siripaci Formations are not present. An equivalent unit to the Cumaná Formation has been identified ('Cumana Formation equivalent unit': CFEU); it is distinct, well exposed and crops out along the ridgeline (Fig. 4a–b). The CFEU is an informal classification termed by this study. It is defined by its two distinct bounding surfaces: a lower erosive contact with apparent down-cut and an upper conformable contact into not well-exposed claystones. It can be correlated to the Cumaná Formation based on the presence of key palynological taxa (i.e. *Retispora lepidophyta* and *Umbellisphaeridium saharicum*). The top of the CFEU is used as a tie-point between log sections (Fig. 4c). The Siripaci Formation is presumed absent under the intra-Carboniferous unconformity (Fig. 3d).

3. Materials, methods and terminology

Sedimentary logs were measured in the field at 1:50 scale using a tape measure and with the aid of a Jacob's Staff and Abney level. The term 'diamictite' is used as a descriptive term that classifies poorly sorted sedimentary rocks with varied grain and clast sizes from clay to boulders (Flint *et al.* 1960a, 1960b). The Moncrieff (1989) classification system is used to discriminate diamictites from other poorly sorted rocks. The classification of Evans *et al.* (2006) was used to interpret diamictite facies.

Fig. 4. (Colour online) Field photographs. (a) Ridgeline. (b) View of the area north of Log A, photo taken at base Log B. (c) View to southeast, photo taken at base Log E. (d) Bioturbation in the Colpacucho Formation at Log A interpreted as *Chondrites* sp. See inset for overlay of bioturbation. (e) Colpacucho Formation sandstones at Log A. (f) Bidirectional cross-stratification and *Skolithos* sp. bioturbation overlain at Log A. (g) Gravelly sandstones in the Cumana Formation Equivalent Unit in Log N with quartz gravel laminae. (h) Strongly cemented gravel bed at Log N. (i) Strongly cemented gravel bed at Log N with details on grooves annotated. (j) Strongly cemented gravel bed, weathered. (k) Log A location with the three diamictite beds annotated. Note the lateral continuity of these beds. Location of (l) and Figure 8g overlain. (l) Inclined and parallel stratification in diamictite facies at Log A. (m) Diamictite with quartz gravel clasts at Log P. (n) Arenite sandstone blocks in diamictite at Log P. (o) Diamictite with soft-sediment sheared clasts at Log A. (p) Metre-scale laminated arenite sandstone blocks at Log I. Scale bar is 5 cm. Field notebook is 13 × 20 cm.

Whole-rock claystone samples were collected from outcrop at a shallow depth (<20 cm). All palynological processing was by standard methods (see Phipps & Playford, 1984), including HCl (37 %) and HF (60 %) followed by decant washing to neutral and sieving at 15 μm. This was followed by a brief short treatment in hot HCl (37 %) to remove neoformed fluorides. The samples were then rapidly diluted into ˜200 ml of water and re-sieved before storing in a vial. Whole kerogen samples were not sieved at 15 μm and directly strewn after HF digestion.

Miospore schemes and index taxa discussed are from western Europe (see Clayton *et al.* 1977; Streel *et al.* 1987; Higgs *et al.* 1988; Maziane *et al.* 1999) and the Amazon Basin, Brazil (see Loboziak *et al.* 1986, 1999, 2000, 2005; Melo & Loboziak 2000, 2003; Loboziak & Melo, 2002; Playford & Melo, 2009, 2012; Melo & Playford, 2012). Biozones are defined on the first occurrences (FOs) of key miospore taxa (Fig. 1). The term 'phytoplankton' refers to the preserved cysts of acritarchs and prasinophytes. Particulate organic matter (POM) includes spore, phytoplankton and phytoclasts (i.e. plant debris) that exist as particulate fragments. Amorphous organic matter (AOM) is structureless under light microscopy and is likely formed in the water column and/or sedimentary substrate via microbial activity (Pacton *et al.* 2011).

Palynological investigation was difficult due to a high degree of degradation typical of the area (see also Díaz-Martinez *et al.* 1999). Only the samples showing the best-preserved palynomorphs were counted to at least 200 specimens for statistical data, with all other samples used for presence/absence data only. Nevertheless, *c.* 75 % of counted specimens could not be identified to a species/generic level or even in open nomenclature. This has likely reduced the total taxon count and imparted a significant preservation bias as: (1) robust forms are likely to have preserved more than fragile ones, and (2) taxa with distinctive features are more readily identified over those with subtle defining characteristics easily obscured by degradation. As mitigation, certain specimens were grouped into larger categories for the relative abundances, such as genera (e.g. *Umbellasphaeridium* spp.) or sculpture characteristics (e.g. apiculate spores).

The carbon content in the samples for the TOC profiles was measured using a Carlo-Erba EA-1108 elemental analyser. Between 2 and 3 mg of both decarbonated and original sample were separately analysed with the machine calibrated using a low Total Carbon (TC) 'soil' standard (1.55 %). Between every 10 samples a check was made using the standard as an unknown.

Organic carbon isotope analysis was undertaken by Iso-Analytical Ltd. They employed an Elemental Analyser – Isotope Ratio Mass Spectrometry (EA-IRMS) technique using a Europa Isotope Ratio Mass Spectrometer. Measurements were calibrated to a wheat flour standard ($\delta^{13}C_{V\text{-}PDB}$ −26.43 ‰) and cross-checked during experimental runs against beet sugar ($\delta^{13}C_{V\text{-}PDB}$ −26.03 ‰) and cane sugar ($\delta^{13}C_{V\text{-}PDB}$ −11.64 ‰) standards. All are calibrated against the international standard IAEA-CH-6 (sucrose, $\delta^{13}C_{V\text{-}PDB}$ −10.43 ‰).

4. Results

4.a. Stratigraphy

4.a.1. Colpacucho Formation

The Colpacucho Formation is at least 560 m thick in Log I, but its basal contact was not observed (Figs 5a and 6). It is composed of claystones that contain siderite concretions and subordinate interbedded sandstones. Larger sandstone interbeds can reach up to 1 m thick, and are cross-bedded, laminated and/or massive with occasional channels. Where preserved (Log A), its uppermost 100 m coarsens upwards into massive, laminated, cross-stratified and/or variably bioturbated sandstones. Bioturbation consists of *Chondrites* sp. with rare *Skolithos* sp. (Fig. 4d–f). The uppermost Colpacucho Formation is defined at the point at which the unit transitions from claystone- to sandstone-dominated. Where the sediment has been significantly bioturbated, there is a mottled texture. At 124–141 m height in Log A, the cross-stratified sandstones contain rare claystone rip-up clasts, gravel laminae and bidirectional cross-stratification (Fig. 4f).

4.a.2. 'Cumaná Formation equivalent unit' (CFEU)

The CFEU varies in thickness from 58 m at Log A to 140 m at Log I. Overall, it is composed of coarse sandstones, gravel and diamictites. Its basal contact is a single or occasionally stacked gravelstone and/or breccia-conglomerate overlying an erosional surface. Variable incision of *c.* 100 m into the underlying bioturbated sandstones of the Colpacucho Formation is inferred from the correlation of sections (Fig. 6a–b). This basal surface marks a subtle yet defining change in sedimentary character, above which sandstones are more thickly bedded, coarser and non-bioturbated. The unit can be broadly split into: (1) a lower sandstone-dominated sub-unit; (2) a laterally and vertically discontinuous, poorly exposed interbedded sub-unit; and (3) an upper sub-unit of cross-laminated sandstones and diamictites (Fig. 6a).

The lower sub-unit is predominantly composed of two facies. The first comprises thickly bedded, cross-stratified and well-sorted medium to coarse grained sandstones. The second comprises matrix-supported and poorly sorted gravelly sandstones that contain gravel and conglomeratic laminae that occasionally overlie erosive scours (Fig. 4g). These facies broadly coarsen upwards.

The interbedded sub-unit consists of cross-laminated sandstones, claystones and laterally restricted poorly sorted purple siltstones and muddy sandstones. The latter are very similar to diamictite facies but lack the coarser sediment fraction and clasts. Hummocky and swaley cross-lamination was observed at 70 m in section Log H. It fines upwards into poorly exposed claystones in Log G (Fig. 6a).

The boundary between the lower and upper sub-units is typically marked by strongly cemented gravel beds that can be correlated between sections (Figs 4h–j and 6a). They have a common stratigraphic association along the ridgeline; they are exclusively found on the top surface of coarsening-upwards gravelly sandstone facies and are always overlain by diamictite (Fig. 7). They are poorly sorted, 5–20 cm thick and contain interspersed quartz gravel that is especially concentrated on the top surface. The top surfaces have a patchy, weathered exposure, and commonly host linear striations and grooves <1 cm deep (Fig. 4h–j).

The upper sub-unit is predominantly composed of diamictites and sandstone facies (Fig. 6a). The diamictites are ≤10 m thick, stratified and matrix-supported clast-rich to clast-poor sandy diamictites. They have relatively straight contacts that are rarely sheared and mostly conformable (Fig. 4k). Exposure is recessive and tends to be obscured by modern soil profiles. Stratification is subtle, defined by colour banding, rare lamination and faint bedding, which can be non-planar (Fig. 4l). The matrix is micaceous, poorly sorted (from clay to gravel) and weathers a distinctive purple colour (Fig. 4m). Clasts are composed of quartz gravel/pebbles (randomly orientated) and arenite sandstone lithics (Fig. 4m–n). A rare number of clasts show soft-sediment shearing (Fig. 4o). Clast size and content is highly variable and diamictites are in
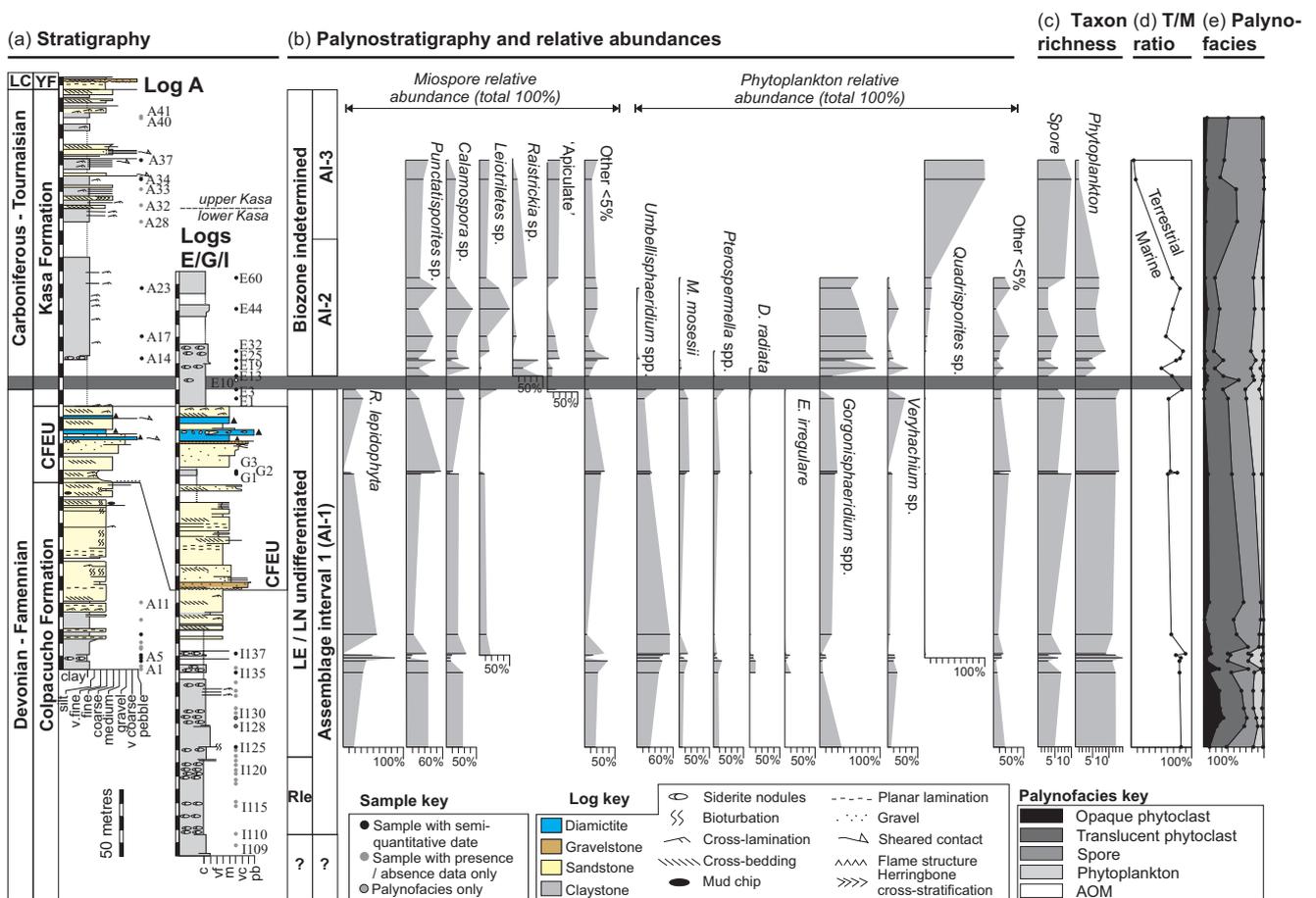
Fig. 5. (Colour online) Composite stratigraphy and palynostratigraphy. Horizontal dark bar is Devonian–Carboniferous boundary interval. (a) Stratigraphy. Columns from left to right are age and formation/unit. White gaps in the logs are gaps in exposure where no log was taken. LC = Late Carboniferous, YF = Yaurichambi Formation, 'CFEU' refers to Cumaná Formation Equivalent Unit. (b) Palynostratigraphy and relative abundances. Columns from left to right are biozones and assemblage intervals (AIs). (c) Taxonomic richness, i.e. number of spore and phytoplankton taxa present. (d) Terrestrial/marine ratio of counted specimens. (e) Palynofacies.

compositional continuity with muddy sandstones where clasts are absent (Fig. 6a). Larger sandstone lithic blocks up to 1 m in diameter were observed in Log I (Fig. 4p). Overturned and convolute laminae are common (Fig. 8a–c). Cross-stratified sandstones are commonly interbedded with the diamictites; either as discrete stringers (<2 cm thick) or as metre-scale beds (Fig. 8d–e). The sandstone facies become progressively more thickly bedded and ripple-marked with height (Figs 7 and 8f). Sheared contacts and convoluted and/or overturned stratification, including flame structures, were observed across the ridgeline but especially at Log A (Fig. 8g–j). Immediately to the southeast of Log A there is a 22 m thick overturned sandstone that lies above the topmost diamictite bed and contained diamictite intraclasts (Fig. 8k–l).

4.a.3. Kasa Formation

The Kasa Formation has a measured thickness of 240 m at Log A. The basal contact is conformable and laterally correlatable. The Kasa Formation is divided into a lower claystone-dominated unit and an upper interbedded unit (Fig. 5a).

The lower unit is *c.* 150 m thick. It is composed of claystones that contain siderite concretionary horizons and interbedded cross-laminated sandstones.

The upper unit is *c.* 90 m thick. Sandstones are cross-stratified, finely interbedded and with rare bioturbation on exposed bed surfaces. There are several thinly interbedded matrix-supported and clast-supported diamictite and conglomerate beds (<1 m thick) that overlie sharp erosive contacts (Fig. 8m). Associated with these are sandstones with overturned laminae and sheaf folds (Fig. 8n–o). The diamictite and conglomerate beds are typically lensoid with limited lateral extent. There is a preferred orientation in the clasts along a sub-horizontal fabric (Fig. 8m – 'Imbricated siderite clasts'). Clasts are well-rounded and primarily composed of siderite nodules and rarer quartz pebbles.

4.b. Palynology

Three palynological assemblage intervals (AIs) are identified. Changes in the miospore and phytoplankton fractions occur at the same stratigraphic levels and are discussed together. See Figures 9 and 10 for palynological plates of the taxa discussed, Table 1 for total assemblage abundances, and the Supplementary Material (available online at https://doi.org/10.1017/S0016756821000741) for the presence/absence data.

4.b.1. Assemblage interval 1: Retispora lepidophyta / Umbellasphaeridium spp.

AI-1 is defined as the range of *Retispora lepidophyta* in the counted samples from sample 'I110' in the Colpacucho Formation to 'E3' in the lowermost Kasa Formation (Fig. 5a–b).
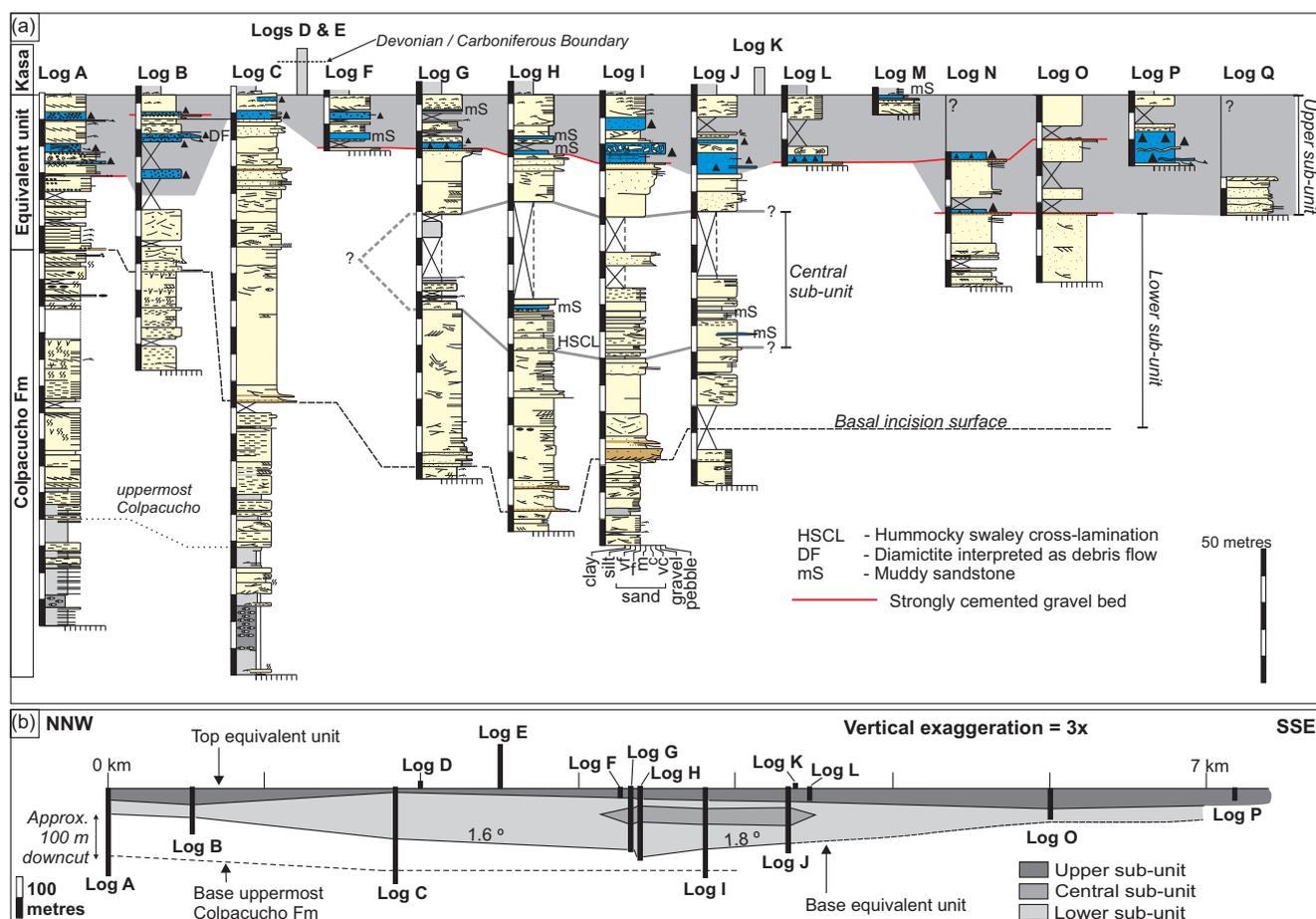
Fig. 6. (Colour online) (a) Measured Logs A–Q through the CFEU. (b) Correlation of logs to lateral scale showing the architecture of the incision surface at 3× vertical exaggeration. See Figure 3c for log locations and Figure 5 for key.

The miospore fraction is relatively poorly preserved, difficult to fully speciate and of low diversity. It is characterized by the high relative abundance of *R. lepidophyta*, which comprises up to a third of the total miospore count. Morphologically simple, single-walled and non-apiculate miospore taxa are common (*Punctatisporites* sp., *Calamospora* sp. and *Leiotrileptes* sp.) and comprise half of the total miospore fraction (Fig. 5b).

Age-diagnostic miospore taxa are rare and were observed in out-of-count presence/absence data only. However, AI-1 does contain the First Occurrences (FOs) of key taxa, such as *Knoxisporites literatus*, *Indotriradites explanatus* and *Verrucosisporites nitidus* (Fig. 5b). Long-lived Devonian and Early Carboniferous species, such as *Densosporites annulatus*, *Emphanisporites rotatus* and *Retusotriletes incohatus*, were also identified.

The phytoplankton fraction has relatively high taxonomic richness and is characterized by the high relative abundance of *Umbellasphaeridium saharicum* and to a lesser extent *Umbellasphaeridium deflandrei* and indeterminate (degraded) *Umbellasphaeridium* sp. (Fig. 5b – '*Umbellasphaeridium* spp.'). There are also common *Gorgonisphaeridium* spp., *Maranhites mosesii*, *Veryhachium trispinosum* group, *Veryhachium lairdii* group, *Pterospermella* spp., *Duvernaysphaera radiata* and *Exochoderma irregulare*. Rare taxa include *Pyloferites pentagonale*, *Stellinium micropolygonale* and *Schizocystia bicornuta*.

4.b.2. Assemblage interval 2: *Gorgonisphaeridium* spp. dominated

The base of AI-2 is defined at the last occurrence (LO) of *R. lepidophyta* in sample 'E3' and is accompanied by an increase in *Gorgonisphaeridium* spp. abundance between samples 'E13' and 'E19' (Fig. 5a–b). The base of AI-2 is also associated with significant reductions in spore and phytoplankton taxonomic richness (Fig. 5c). The interval is entirely constrained within the lower unit of the Kasa Formation (Fig. 5b).

The miospore fraction is dominated by the morphologically simple, single-walled and non-apiculate *Punctatisporites* sp., *Calamospora* sp. and *Leiotrileptes* sp. genera, which comprise >60 % of the total miospore count. There is a relative increase in single-walled apiculate miospores: *Anapiculatisporites* sp., *Apiculatisporites* sp., *Apiculiretusispora* sp. (Fig. 5b – 'apiculate') and *Raistrickia* sp. (Fig. 5b – '*Raistrickia*').

Age-diagnostic miospore taxa are extremely rare, and difficult to speciate with confidence. Only a single age-diagnostic species, *Anapiculatisporites semicuspidatus*, had its FO within AI-2.

The phytoplankton fraction is relatively impoverished compared to AI-1 and characterized by the high relative abundance of *Gorgonisphaeridium* spp., which accounts for 73 % of total identified phytoplankton. AI-2 is also associated with the long-lived Palaeozoic to Mesozoic phytoplankton genera *Veryhachium*
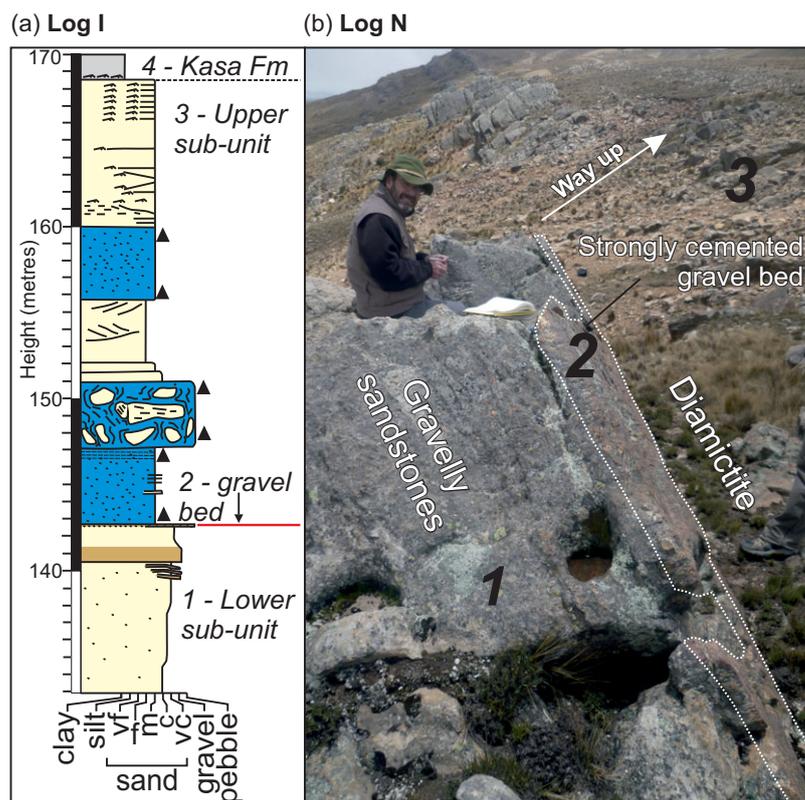
Fig. 7. (Colour online) Stratigraphic association of the strongly cemented gravel beds at (a) Log I and (b) Log N. These logs are laterally separated by 1200 m.

spp., *Micrhystridium* spp. and *Quadrisporites* sp. These are minor components of AI-2, but their relative abundances are relatively unchanged from the preceding AI-1 (Fig. 5b). Those taxa which disappear entirely into AI-2 include *E. irregulare*, *Gorgonisphaeridium winslowiae*, *Schizocystia bicornuta*, *Stellinium comptum* and *Stellinium* sp. The following taxa persist into AI-2, but in extremely reduced numbers: *D. radiata*, *Horologinella quadrispina*, *Lophosphaeridium* sp., *M. mosesii*, *Pterospermella* spp., *P. pentagonale*, *Stellinium micropolygonale*, *U. deflandrei* and *U. saharicum*.

4.b.3. Assemblage interval 3: spore-dominated

The base of AI-3 is defined at the loss of the phytoplankton fraction (including *Gorgonisphaeridium* spp.) in sample 'A34' (Fig. 5b–d). It is spore- and phytoclast-dominated and ranges entirely within the upper Kasa Formation.

The miospore fraction is difficult to identify confidently due to poor preservation. However, *Punctatisporites* sp., *Leiotriletes* sp. and *Calamospora* sp. were common and comprise 49 % of the total miospore count. The rest are mostly single-walled apiculate genera such as *Anapiculatisporites* sp., *Apiculatisporites* sp., *Apiculiretusispora* spp., *Claytonispora* sp. and *Raistrickia* sp.

The following age-diagnostic miospore taxa had their FOs in AI-3 but are either extremely rare or limited to single occurrences. These are: *Anapiculatisporites ampullaceus*, *Indotriradites dolianitii* morphon, *Indotriradites viriosus* and *Waltzispora lanzonii*. Only a single specimen of *W. lanzonii* that conformed to its original type description was identified (see Daemon, 1974). Several unusual forms were observed with up to four poorly developed apical shoulders, which are comparable to those described by Playford & Melo (2010, 2012). *Waltzispora* sp. 1 is morphologically like *W. lanzonii* but lacks shoulder apiculation. Additional age-diagnostic

species have their FOs within AI-3 but are known from the Late Devonian. These include: *Aratrisporites saharaensis*, *Convolutispora major*, *Verrucosisporites congestus* and *Verrucosisporites depressus* (Playford & Melo, 2012).

Phytoplankton are almost non-existent in AI-3. Only rare specimens of *Quadrisporites* sp. were observed in the counts. Specimens of other marine phytoplankton taxa were only sporadically observed in the presence/absence data.

4.b.4. Palynofacies

The palynofacies are dominated by terrestrially derived phytoclasts and spores, with only minor proportions of marine phytoplankton and amorphous organic matter (AOM) (Fig. 5e). Some broad trends are recognized. There is an upwards decrease in the relative abundance of the marine fraction ('phytoplankton' and 'AOM') in the uppermost Colpacucho Formation. The proportion of phytoclasts in the lower Kasa Formation (AI-2) is reduced. In contrast, there is a sudden increase in phytoclast content in the upper Kasa Formation (AI-3), coincident with the decrease in Terrestrial/Marine (T/M) ratio in the counts.

4.c. TOC and $\delta^{13}C_{organic}$

4.c.1. Colpacucho Formation

Total organic carbon values typically vary between 0.3 and 1.5 %, but peak at 2.5 % in sample A-10, which is coincident with an increase in phytoclast content (Fig. 11).

Only those samples above the FO of *Indotriradites explanatus* (LE/LN zone) were processed for bulk $\delta^{13}C_{org}$ as this is the level in which global PCIEs have been observed (Fig. 11; see also Kaiser *et al.* 2016). $\delta^{13}C_{org}$ values are variable within a *c.* 1 ‰ range (−24.3 to −25.16 ‰), with a mean average of −24.27 ‰.

Fig. 8. (Colour online) Field photographs. (a) Convolute laminae in diamictite at Log F. (b) Overturned laminae in diamictite at Log F. (c) Convolute laminae and possible water-escape structures in diamictite at Log F. (d) Interbedded thin sandstones in diamictite. (e) Sandstone channel in diamictite at Log P. (f) Ripple-marked sandstone at near top CFEU. (g) Sheared sandstones in CFEU at Log A. Locations of (h–i) overlain. (h) Overturned laminae in sandstones. See (g) for location. (i) Soft-sediment deformation and sheared basal contact. See (g) for location. (j) Flame structure in CFEU sandstones at Log A. (k) Slump structure at top CFEU at Log A. (l) Slump structure annotated showing position above a diamictite décollement. (m) Laterally restricted debris flow with imbricated siderite clasts in the Kasa Formation at Log A. (n) Overturned laminae in forming a sheaf fold in the Kasa Formation at Log A. (o) Closer photo of overturned laminae in (n). Scale bar is 5 cm.
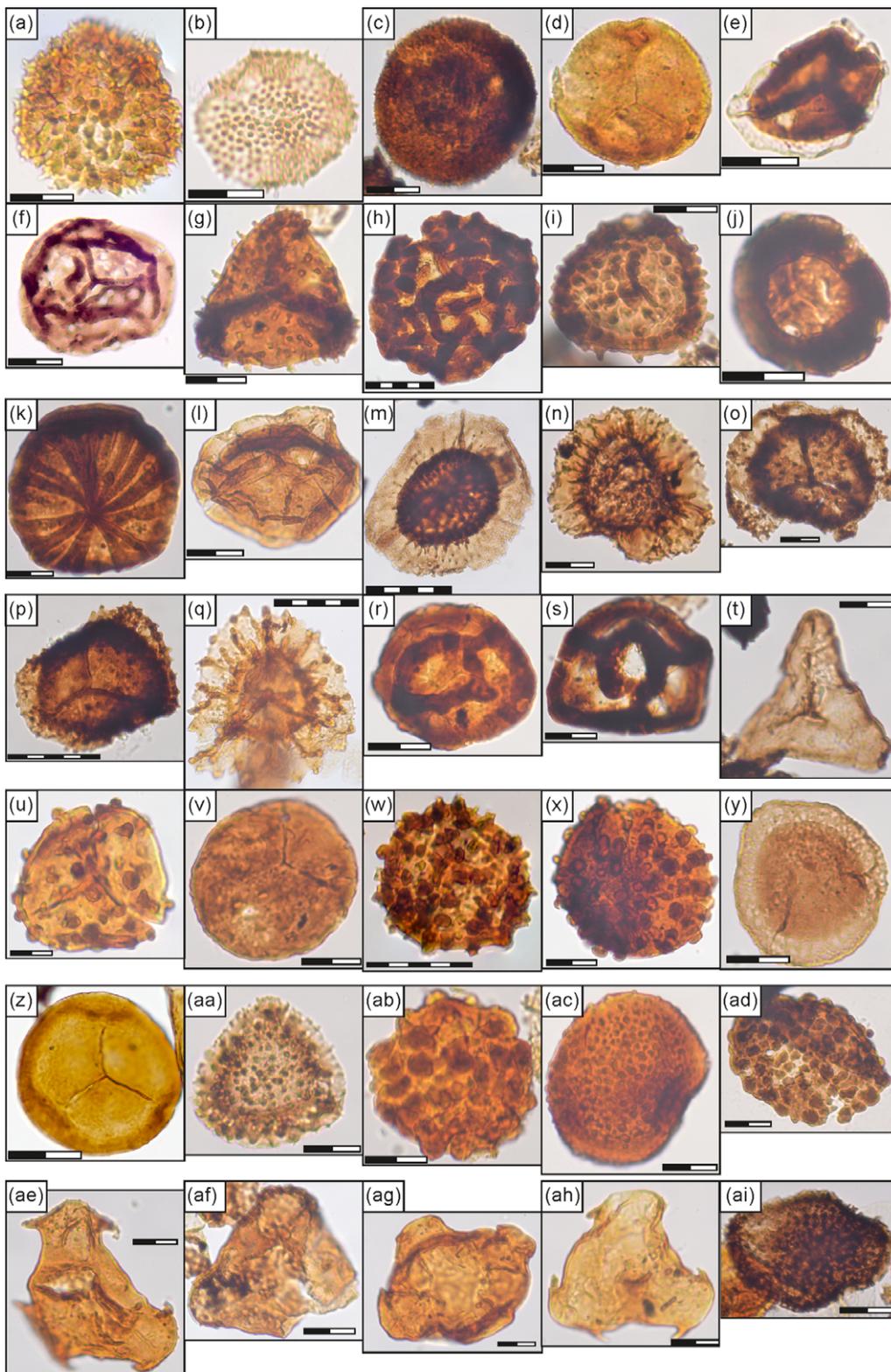
Fig. 9. (Colour online) Palynological plate 1: miospores. Scale bars are 20 μm and 50 μm. (a) *Anapiculatisporites ampullaceus.* (b) *Anapiculatisporites semicuspidatus.* (c) *Apiculatisporites quadrosii.* (d) *Apiculiretusispora* sp. (e) *Auroraspora* sp. (f) *Calamospora* sp. (g) *Claytonispora* sp. (h) *Convolutispora major.* (i) *Cymbosporites* sp. (j) *Densosporites annulatus.* (k) *Emphanisporites rotatus.* (l) *Endosporites angustus.* (m) *Grandispora protea.* (n) *Indotriradites dolianitii* morphon. (o) *Indotriradites explanatus.* (p) *Indotriradites explanatus.* (q) *Indotriradites viriosus.* (r) *Knoxisporites literatus.* (s) *Knoxisporites literatus.* (t) *Leiotrileterotus* sp. (u) *Neoraistrickia* sp. (v) *Punctatisportites* spp. (w) *Raistrickia* sp. (x) *Raistrickia* sp. (y) *Retispora lepidophyta.* (z) *Retusotriletes incohatus.* (aa) *Vallatisporites* sp. (ab) *Verrucosisporites congestus.* (ac) *Verrucosisporites depressus.* (ad) *Verrucosisporites nitidus.* (ae) *Waltzispora lanzonii.* (af) *Waltzispora lanzonii* aberrant. (ag) *Waltzispora lanzonii* aberrant. (ah) *Waltzispora* sp. 1. (ai) *Aratrisporites saharaensis.*
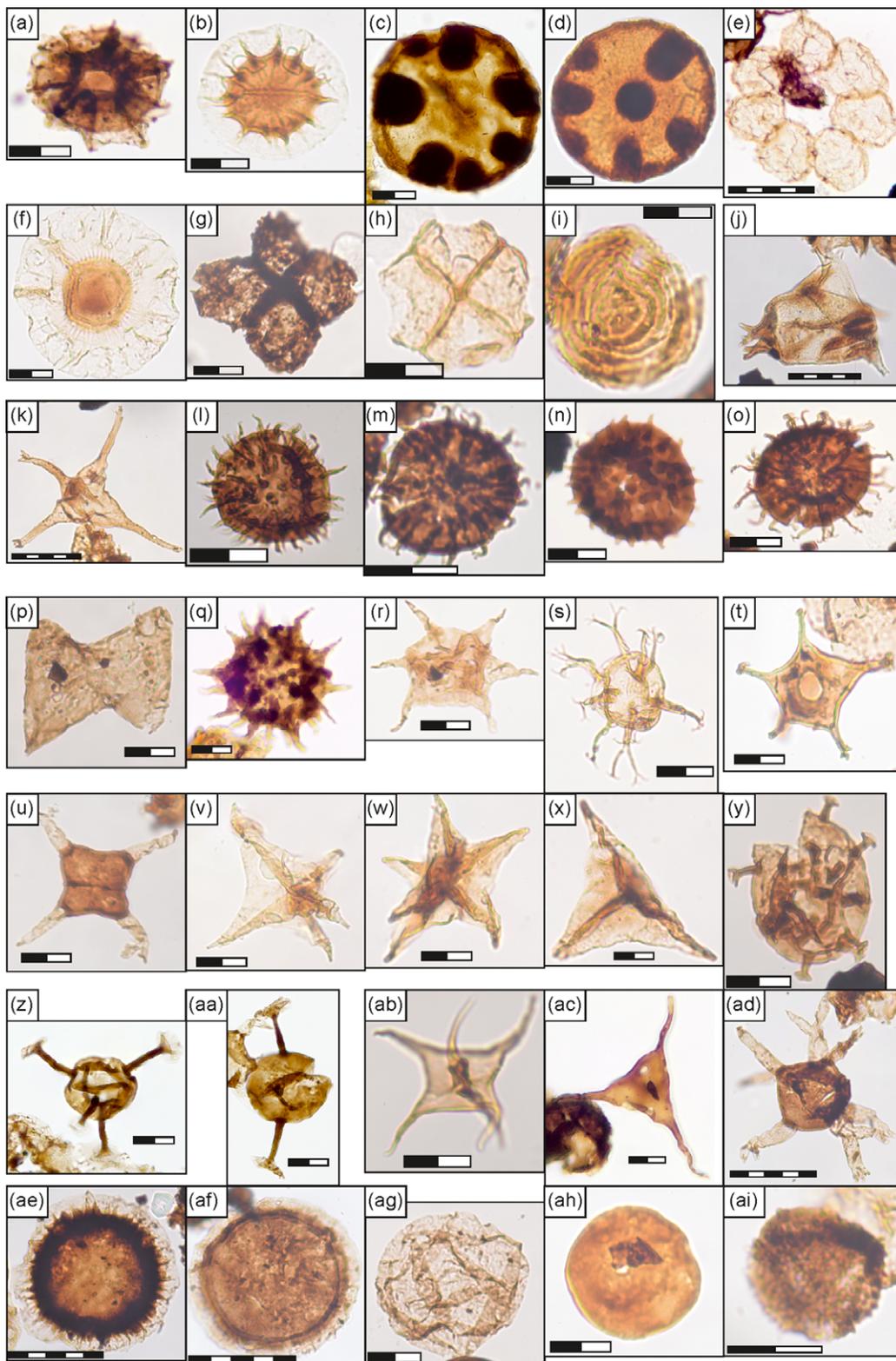
Fig. 10. (Colour online) Palynological plate 2: Acritarchs and prasinophytes. (a) *Cymatiosphaera ambotrocha.* (b) *Duvernaysphaera radiata.* (c) *Maranhites mosesii.* (d) *Maranhites mosesii.* (e) *Petrovina connata.* (f) *Pterospermella* spp. (*P. pernambucensis*). (g) *Quadrisporites* sp. (h) *Quadrisporites* sp. (i) *Chomotriletes vedugensis.* (j) *Evittia sommeri.* (k) *Exochoderma irregulare.* (l) *Gorgonisphaeridium* spp. (m) *Gorgonisphaeridium* spp. (n) *Gorgonisphaeridium* spp. (o) *Gorgonisphaeridium winslowiae.* (p) *Horologinella quadrispina.* (q) *Micrhystridium breve* group. (r) *Micrhystridium pentagonale* group. (s) *Multiplicisphaeridium ramusculosum.* (t) *Pyloferites pentagonale.* (u) *Schizocystia bicornuta.* (v) *Stellinium comptum.* (w) *Stellinium micropolygonale.* (x) *Stellinium* sp. 1. (y) *Umbellasphaeridium deflandrei.* (z) *Umbellasphaeridium saharicum.* (aa) *Umbellasphaeridium saharicum.* (ab) *Veryhachium lairdii* group. (ac) *Veryhachium trispinosum* group. (ad) Incertae sedis 1. (ae) Incertae sedis 2. (af) Incertae sedis 2. (ag) *Leiosphere* sp. (ah) *Leiosphere* sp. (ai) *Lophosphaeridium* sp.

Table 1. Total relative abundance by all samples in each assemblage interval.

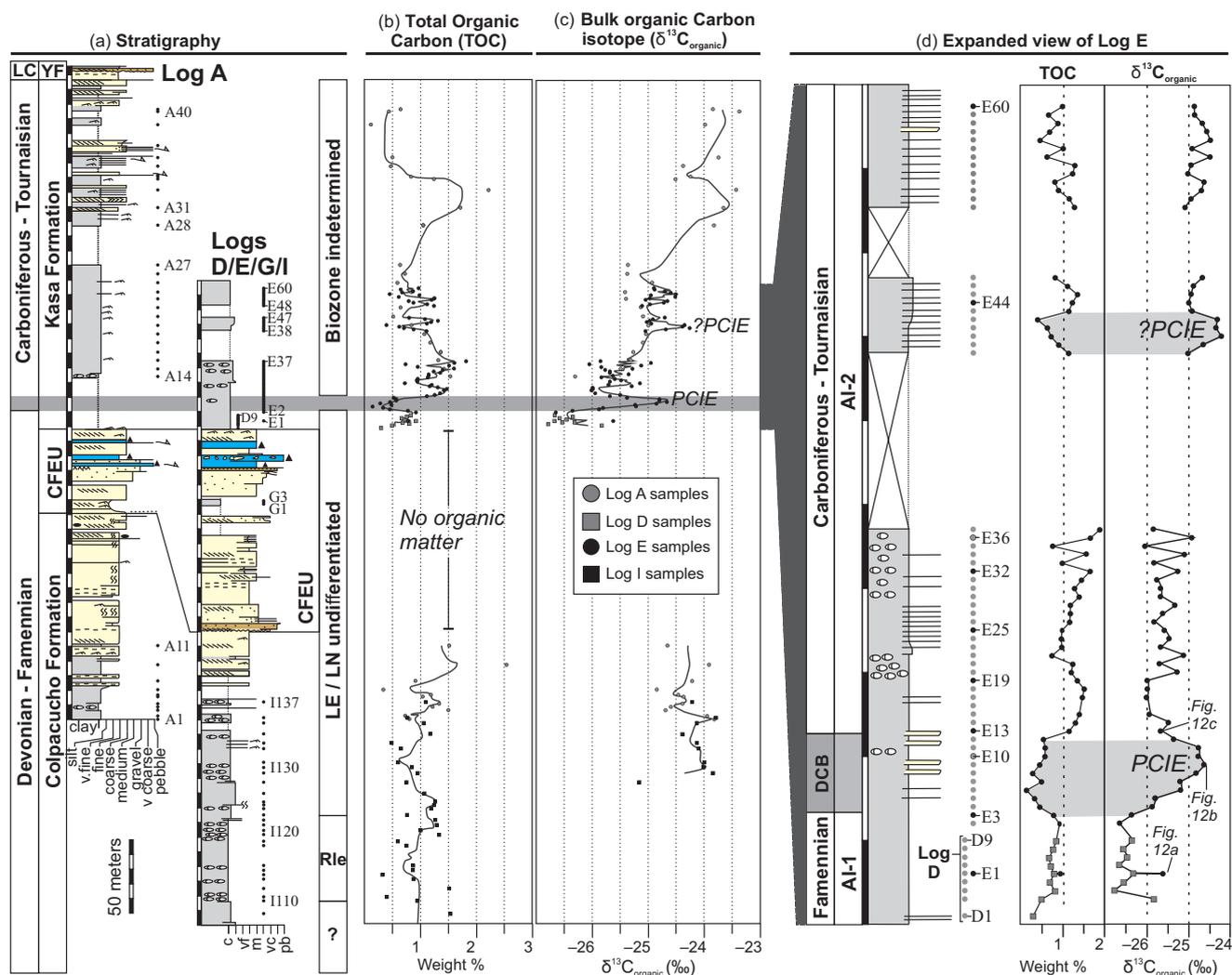| Spore total relative abundance by assemblage						Phytoplankton relative abundance by assemblage					
Assemblage 1	%	Assemblage 2	%	Assemblage 3	%	Assemblage 1	%	Assemblage 2	%	Assemblage 3	%
R. lepidophyta	32	*Punctatisporites* sp.	32	*Punctatisporites* sp.	33	*Umbellisphaeridium saharicum*	27	*Gorgonisphaeridium* spp.	73	*Quadrisporites* sp.	100
Punctatisporites sp.	23	*Calamospora* sp.	18	*Leiotriletes* sp.	17	*Gorgonisphaeridium* spp.	14	*Veryhachium trispinosum* group	7		
Calamospora sp.	19	*Raistrickia* sp.	18	*Apiculatisporites* sp.	11	*Maranhites mosesii*	10	*Quadrisporites* sp.	5		
Leiotriletes sp.	7	*Leiotriletes* sp.	12	*Retusotriletes* sp.	10	*Pterospermella* spp.	9	*Micrhystridium breve* group	4		
Indotriradites sp.	4	*Convolutispora* sp.	6	*Calamospora* sp.	8	*Umbellisphaeridium deflandrei*	9	*Micrhystridium pentagonale* group	2		
Cymbosporites sp.	3	*Apiculiretusispora* sp.	4	*Anapiculatisporites* sp.	6	*Veryhachium trispinosum* group	8	*Maranhites mosesii*	2		
Retusotriletes incohatus	2	*Anapiculatisporites* sp.	3	*Apiculiretusispora* sp.	4	*Duvernaysphaera radiata*	5	*Muraticavea* sp.	2		
Densosporites annulatus	1	*Apiculatisporites* sp.	3	*Raistrickia* sp.	3	*Exochoderma irregulare*	3	*Veryhachium lardii* group	1		
Emphanisporites rotatus	1	*Retusotriletes* sp.	2	Other (≤ 1 %)	8	*Gorgonisphaeridium winslowiae*	3	*Leiosphere* sp.	1		
Apiculiretusispora sp.	1	Other (≤ 1 %)	3			Incertae sedis: 1	2	*Pterospermella* spp.	1		
Auroraspora sp.	1					*Multiplicisphaeridium* sp.	2	*Stellinium micropolygonale*	1		
Grandispora sp.	1					*Leiosphere* sp.	2	*Umbellisphaeridium saharicum*	1		
Other (≤ 1 %)	5					*Veryhachium lardii* group	2	Other (<1 %)	1		
						Pyloferites pentagonale	1				
						Lophosphaeridium sp.	1				
						Stellinium micropolygonale	1				
						Quadrisporites sp.	1				
						Other (<1 %)	2				
N = 220		*N* = 109		*N* = 72		*N* = 640		*N* = 241		*N* = 2	

Fig. 11. (Colour online) Geochemistry. Horizontal dark bar is DCB interval. (a) Stratigraphy – see Figure 5 for key. (b) Composite total organic carbon with three-point average curve. (c) Composite δ¹³C$_{organic}$ with three-point average curve. (d) Expanded view of Logs D and E showing 2 ‰ PCIE in a continuous run of samples through the DCB.

4.c.2. Lower Kasa Formation

TOC averages 0.95 %. Trends appear negatively correlated with δ¹³C$_{org}$, but there is no overall statistical relationship ($R^2 = 0.02$).

There is a negative shift in bulk δ¹³C$_{org}$ values of *c.* 2 ‰ compared to the uppermost Colpacucho Formation. There is an upwards positive trend throughout the lower Kasa Formation (samples D1 to A27) of 1.6 ‰. Within this trend there is at least one PCIE, and potentially two. These are more clearly observed in Logs D and E where there are near-continuous runs of samples at 1 m intervals (Fig 11f).

The lower 2 ‰ PCIE is at 13–22 m above the base lower Kasa Formation and is coincident with a negative TOC excursion of 0.8 %. Its base (sample E3) contains the last counted occurrence of *Retispora lepidophyta*. Particulate organic matter is noticeably darker and more degraded in samples through the 2 ‰ PCIE compared to those above and below (Fig. 12). Immediately above the PCIE, both TOC and bulk δ¹³C$_{org}$ increase by *c.* 1 % and 1 ‰ respectively. This is accompanied by less degraded and more translucent POM and the lowest observation of AI-2 (Figs 5 and 12c).

Processed palynological recovery was sparse through the 12–22 m interval in Log E (2 ‰ PCIE), despite the average TOC values of

0.52 %. This suggests that the bulk of the organic residue in the PCIE samples was in the <15 μm fraction lost during standard palynological processing (i.e. washed through the 15 μm nylon mesh). To investigate further, those palynological samples between 13 and 22 m height in Log E were reprocessed using HF only and with the <15 μm fraction retained. The resulting residues contained AOM and neoformed fluorides (the latter a consequence of HF reacting with clay minerals and trace calcium in the sample). This means that AOM was preferentially lost during palynological processing.

The second PCIE (1 ‰) is at 68–72 m in Log E and is accompanied by a negative TOC excursion of 0.7 %. However, due to the break in section at 47–68 m height it is only partially sampled (Fig. 11).

4.c.3. Upper Kasa Formation

TOCs and bulk δ¹³C$_{org}$ increase markedly into the upper Kasa Formation to a maximum of 2.2 % and −23.9 ‰ respectively. This correlates with the total loss of the marine fraction and the increase in phytoclast content observed in AI-3 (Fig. 11). In the upper part, TOCs decrease to an average of 0.6 %.
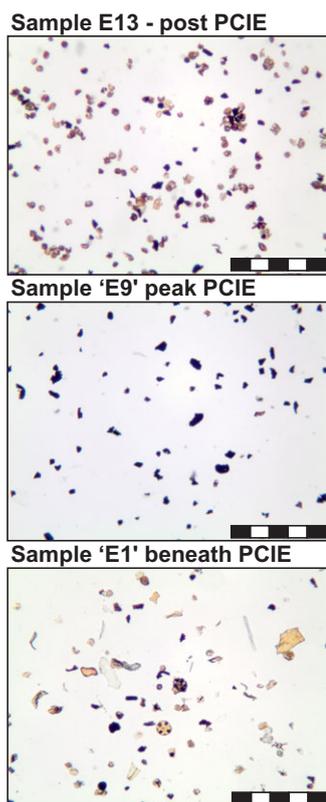
Sample E13 - post PCIE

Sample 'E9' peak PCIE

Sample 'E1' beneath PCIE

Fig. 12. (Colour online) Palynological assemblages in samples E1, E9 and E13 that were processed through standard techniques. Samples E1 and E13 are beneath and above the 2 ‰ PCIE respectively. Sample E9 is at the peak of the 2 ‰ excursion and shows much more degraded and darkened POM compared with those samples E1 and E13. Scale bars are 500 μm.

5. Interpretation

5.a. Depositional history

5.a.1. Colpacucho Formation: open-marine

The Colpacucho Formation is an open-marine shelf environment based on the phytoplankton population observed in AI-1 and previous work (Díaz-Martínez, 1991). The claystone-dominated lower part is interpreted as offshore. The uppermost Colpacucho is interpreted as a prograding shoreface (Fig. 13a). The high degree of bioturbation in the shoreface sands suggests environmental conditions were either more favourable for biological life or allowed for greater preservation potential. An absence of body fossils, spreite and back-fill structures suggests that bioturbation was caused by soft-bodied organisms, such as annelid or nematode worms. Tidal processes are interpreted to explain claystone rip-up clasts, gravel laminae and bidirectional cross-stratification at the very top of the Colpacucho Formation at Log A (Figs 4f and 5a–b). These results indicate a shallowing-upwards trend and transition from an offshore marine environment into a tidally influenced shoreface. This is reflected in the decrease in marine palynomorphs in the palynofacies counts (Fig. 5e).

5.a.2. Cumaná Formation Equivalent Unit (CFEU): glaciomarine and remobilization

The CFEU is interpreted as glacigenic based on the following criteria: (1) striations and grooves, (2) diamictites containing large lithic blocks, (3) sheared contacts and soft-sediment deformation, (4) sandstone stringers and channels interpreted as ice–bed separation and (5) the association between striations/grooves and diamictites, where the former are exclusively overlain by the latter. Furthermore, the palynology present (Section 4.b.1) confirm its equivalence to the regional and glacigenic Cumaná Formation (Díaz-Martínez & Isaacson, 1994; Díaz-Martínez et al. 1999) and global context of glacial diamictites (Lakin et al. 2016). Marine conditions are supported by the occurrence of the same phytoplankton assemblage in samples below, within, and above the unit (Fig. 5b).

The basal surface represents a major erosional event associated with c. 100 m of incision into the underlying shoreface sands (Fig. 13b). There is no evidence for direct ice contact at the base of the CFEU (no striations/diamictites, etc.). The simplest hypothesis is subaerial or submarine erosion following sea-level fall in the preceding Colpacucho Formation (Section 5.a.1).

The lower sub-unit is interpreted as a subaqueous proglacial fan system, analogues of which contain common coarse massive to cross-stratified sandstones (e.g. Hornung et al. 2007) (Fig. 13c). The coarsening-upwards trends are interpreted as the progradation of proglacial fans and ice advance. Rare, overturned beds (such as at c. 30 m height in Log G) are interpreted as soft-sediment deformation caused by rapid deposition and excess pore pressure (Talling et al. 2012). Grain-size segregation into gravelly and conglomeratic laminae may have taken place during flow separation (Carling, 1990).

The interbedded sub-unit is relatively distal, as shown by claystone facies (Fig. 13c). Poorly sorted muddy and silty sandstones are rare and are interpreted as thin debris flows. The hummocky–swaley cross-stratification shows evidence of storms. The AI-1 palynology indicates that offshore marine conditions and terrestrial vegetation were unaffected by the advance of ice both regionally and globally. Interestingly, these facies do not contain dropstones, which contrasts with the dropstone-in-shale deposits typical of the Cumaná Formation (Díaz-Martínez & Isaacson, 1994). Assuming a glacigenic interpretation is correct, there are two possibilities: (1) there was a localized ice retreat in the study area; or (2) glaciers in the study area did not contain much lithified and/or exotic clast material.

The striated/grooved gravel beds, which typically mark the boundary between the lower and upper sub-units, are interpreted as subglacial ice traction onto soft sediment. Gravel would have been deposited via lodgement processes. Their consistent stratigraphic position at the top of coarsening-upwards gravel sandstones is interpreted to mark the point at which proglacial sands were overridden by the advancing ice sheet. No deformational structures were observed beneath the striations and grooves. Subglacial drainage may have lubricated the basal surface and inhibited the formation of glacio-tectonized structures. Alternatively, subglacial ductile shearing and/or ice-keel scouring can also form soft-sediment striations without deformation (Woodworth-Lynas & Dowdeswell, 1994; Le Heron et al. 2005; Vesely & Assine, 2014). However, no features typical of these mechanisms (i.e. stacked striated pavements or scour/berm structures) were identified and so an ice-traction hypothesis is preferred. A non-glacial interpretation is also considered unlikely. The striations and grooves do not conform to typical definitions of tool marks and gutter casts, which are moulds or casts caused by erosion beneath a coarser unit into unconsolidated muddy sediment (see Middleton, 2003; Myrow, 2003)

The upper sub-unit is interpreted as subglacial (Fig. 13d). The diamictite facies mostly contain randomly orientated clasts and gravel, suggesting that lodgement processes were predominant. However, the presence of sheared sandstone clasts and overturned laminae suggests a mixture of both deformational and lodgement
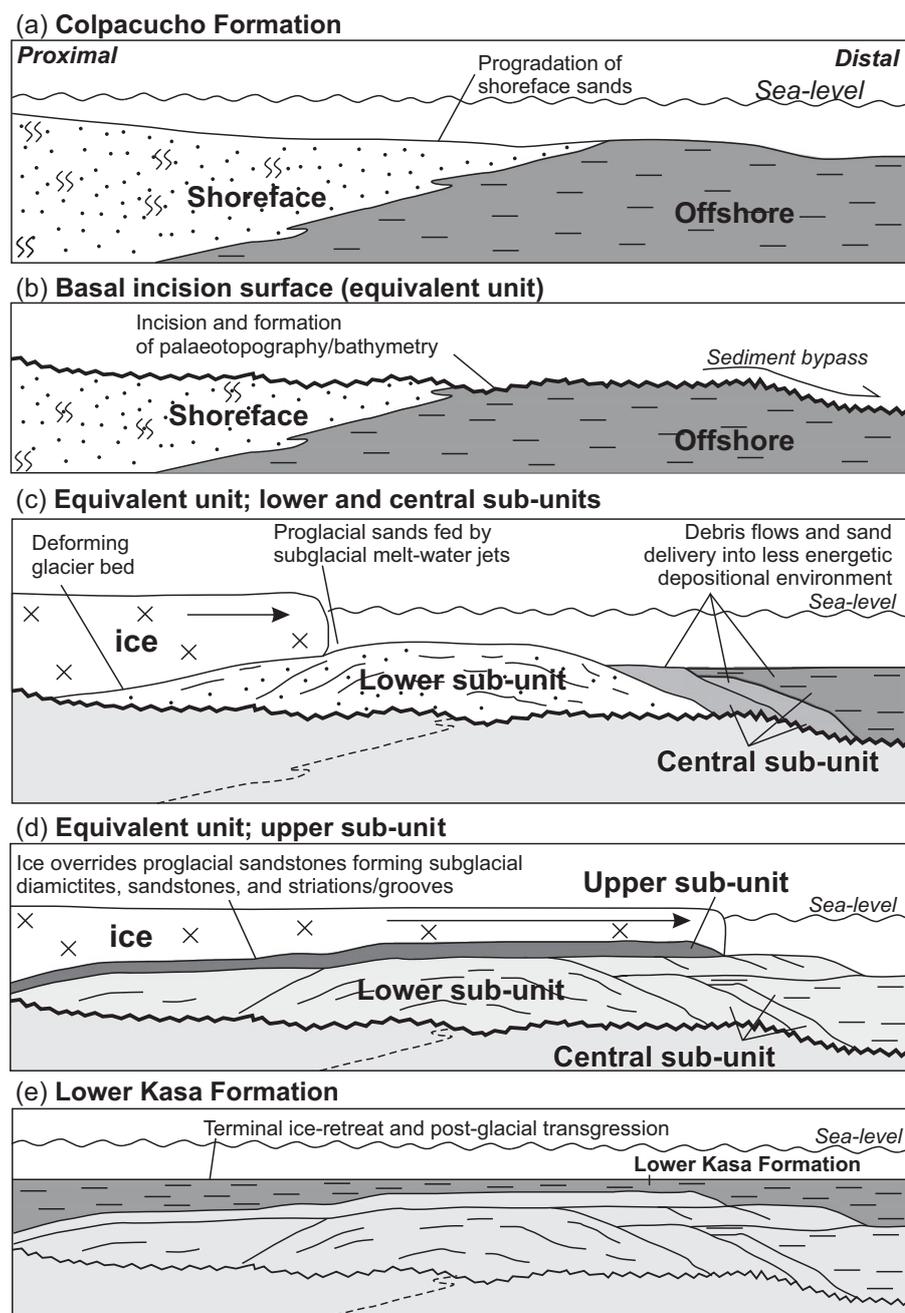
Fig. 13. Depositional model. (a) Colpacucho Formation: prograding shoreface. (b) Cumaná Formation Equivalent Unit (CFEU): basal incision surface. (c) CFEU: proglacial lower and central sub-units. (d) CFEU: subglacial upper sub-unit. (e) Lower Kasa Formation: post-glacial transgression.

processes. Lithic clasts were probably reworked from the underlying and interbedded sandstones due to their compositional similarity. Sandstone stringers and lenses within the diamictite beds are interpreted to have been deposited by basal melt-water films formed via ice–bed separation (see Piotrowski *et al.* 1999, 2001). Overturned laminae in these sandstones are evidence for post-depositional remobilization. Subglacial drainage may explain the presence of larger, stratified sandstone beds (Evans *et al.* 2006). The 'ice-traction till' classification of Evans *et al.* (2006) incorporates a continuum of deformational and lodgement depositional features and stratified inter-diamictite sandstones that is comparable to the features described in the CFEU. The overturned 22 m unit near Log A is interpreted as localized slumping above a diamictite décollement. Convoluted laminations and flame structures at Log A are further evidence of remobilization and dewatering.

5.a.3. Kasa Formation: open-marine to pro-deltaic

The 239 m directly measured thickness at Log A is significantly less than the 600–1400 m reported regionally (Díaz-Martínez, 1991, 1993). Sedimentation rates could have been reduced here, or, more likely, it was eroded during the development of the overlying intra-Carboniferous unconformity.

The lower unit is interpreted as offshore marine. The basal contact is straight, sharp and widely correlated, suggesting sudden retrogradation of the preceding CFEU as ice receded and the climate warmed (Fig. 13e).

The upper unit records the progradation of relatively proximal sandstone facies. This is a common regional trend and is interpreted as the progradation of deltaic systems onto a shelfal setting (Díaz-Martínez, 1991, 1993; Díaz-Martínez & Isaacson, 1994; Díaz-Martínez *et al.* 1999; Isaacson *et al.* 2008). In this study,

the lensoid conglomerates/diamictites, erosive contacts, overturned laminae, sheaf folds and siderite rip-up clasts are interpreted as reworked density flows and debrites in an inclined pro-delta or delta-front setting. Siderite rip-up clasts are likely to have been derived from claystone deposits up-dip.

In other studies, conglomerates and diamictites in the Kasa Formation are thought to have been triggered by proglacial outbursts during an early Carboniferous glaciation event (Díaz-Martínez & Isaacson, 1994; Isaacson *et al.* 2008). This is supported by evidence for two Early Carboniferous glacial events in western Gondwana in the Tournaisian and Viséan (Caputo *et al.* 2008; Lakin *et al.* 2016). Ice may have persisted above the CFEU up-dip from the study area. However, there are no independent ice indicators (i.e. dropstones, striations, etc.) observed to support this in Log A and so a reworking interpretation is preferred.

5.b. Age and palynostratigraphy

5.b.1. Assemblage interval 1 – latest Famennian

Assemblage interval 1 (AI-1) has relatively diverse miospore and phytoplankton populations that indicate open-marine conditions (Fig. 5c–d).

Retispora lepidophyta has a near-global extent in the latest Famennian and is an important index species owing to its short geologic range and distinctive morphology (Maziane *et al.* 2002). As the vertical range of AI-1 is concurrent with *R. lepidophyta* it is interpreted to represent the latest Famennian Stage (Devonian). An undifferentiated LE/LN zone is defined from the FO of *Indotriradites explanatus* to the LO of *R. lepidophyta* (Fig. 5b). Further biostratigraphic refinement is not possible due to the extremely rare occurrence of key taxa, including *Verrucosisporites nitidus*. This spore is also noted to be rare in the Amazon Basin (Playford & Melo, 2012) and has been reinterpreted in western Europe as an ecozone representing proximal environments (Prestianni *et al.* 2016). It may therefore not be a suitable marker species for age correlation. The Amazon Basin RLe/LVa zones could not be recognized due to the relative paucity and poor preservation of *Vallatisporites* sp. specimens.

A latest Famennian age is also supported by *Umbellasphaeridium saharicum*, a distinctive Famennian acritarch (Jardiné *et al.* 1974; Díaz-Martínez *et al.* 1999; Vavrdova & Isaacson, 1999; Wicander *et al.* 2011). Its occurrence defines an endemic 'Phytoplankton Bioprovince' restricted to Gondwana and the southern margin of Euramerica (Vavrdova & Isaacson, 1999). The bioprovince is commonly associated with *Pyloferites pentogonale*, *Maranhites mosesii*, *Horologinella quadrispina*, *Pterospermella* spp., *Duvernaysphaera radiata* and *Stellinium micropolygonale*, which are common taxa recognized in AI-1.

5.b.2. Identifying the Devonian/Carboniferous Boundary

The extinction of *R. lepidophyta* is near-synchronous with the DCB as currently defined (see Higgs & Streel, 1993; Aretz *et al.* 2016). As such, the DCB is picked on the last counted occurrence of *R. lepidophyta* (Fig. 5a). Very rare occurrences of *R. lepidophyta* were observed above the picked DCB in the presence/absence data and are interpreted as reworked (see Supplementary Material available online at https://doi.org/10.1017/S0016756821000741). Reworked *R. lepidophyta* is not unusual and this has been described in Mississippian strata of the Amazonas Basin (Melo & Playford, 2012).

The significant loss of phytoplankton taxonomic richness and assemblage overturns between AI-1 and AI-2 represents EDME as expressed in the high-palaeolatitude record (Fig. 5b–d). The miospore (terrestrial) and phytoplankton (marine) overturns occur synchronously and abruptly in the initial post-glacial marine transgression.

In the miospore fraction, the relative abundance increases of apiculate miospores immediately above the DCB suggest the ecological niche that *R. lepidophyta* occupied was almost immediately filled post-extinction. The long-lived and morphologically simple genera *Punctatisporites* sp., *Leiotrileptes* sp. and *Calamospora* sp. were apparently unaffected.

In the phytoplankton fraction, the DCB is clearly marked by the loss of the Late Devonian '*U. saharicum*' bioprovince (Vavrdova & Isaacson, 1999). Those acritarch genera least affected, *Gorgonisphaeridium*, *Veryhachium* and *Micrhystridium*, are morphologically simple, long-lived and range through the Phanerozoic (Sarjeant & Stancliffe, 1994; Servais *et al.* 2007). The dominance of *Gorgonisphaeridium* spp. in AI-2 suggests it was an opportunistic disaster taxon post-EDME.

5.b.3. Assemblage intervals 2 and 3 – Tournaisian

AI-2 is an impoverished assemblage dominated by long-lived spore and acritarch genera with simple morphologies, reflecting a post-EDME setting. AI-3, in contrast, is likely a depositional effect caused by the progradation of coarser terrigenous material in the upper Kasa Formation. This is supported by the palynofacies being almost entirely composed of terrestrially derived phytoclasts and spores. Those Late Devonian to Carboniferous spores whose FOs occur in AI-3 are either reworked or are more likely to be observed in the relatively proximal facies of the upper Kasa Formation.

AI-2 and AI-3 are undifferentiated Tournaisian Stage (Carboniferous) based on the FOs of the miospores *Anapiculatisporites semicuspidatus*, *Indotriradites viriosus* and single occurrence of *Waltzispora lanzonii* in A-23, A35 and A-33 respectively. These taxa are restricted to the Tournaisian AL-PD miospore zones in the Amazon Basin (Fig. 1; Melo & Playford, 2012; Playford & Melo, 2012). Although Playford and Melo (2010) discussed the possibility that *W. lanzonii* extends into the Viséan, they considered the few records in this stage to be more likely due to reworking. Díaz-Martínez *et al.* (1999) observed *Dibolisporites distinctus* (now *Claytonispora distincta*) and *Raistrickia clavata* in the Kasa Formation at the Log A road section. These species were not identified in this study, but their presence would suggest that mid- to late Tournaisian (PC/PD zones) sediments are present.

5.c. Chemostratigraphy

5.c.1. Potential controlling factors

The global correlation of PCIEs at or around the DCB in both organic and inorganic carbon implies a global mechanism. Widespread marine anoxia and organic carbon burial is the leading hypothesis (Kaiser *et al.* 2016). Bulk $\delta^{13}C_{org}$ data (as in this study) reflect the sum value of all organic matter from the rock sample, including both terrestrial (spores, phytoclasts) and marine (phytoplankton cysts, water-column derived AOM) sources. This is important as stratigraphic trends in bulk $\delta^{13}C_{org}$ can be influenced by processes that favour the delivery (and preservation) of marine or terrestrial organic matter (Davies *et al.* 2012; Könitzer *et al.* 2014).

Furthermore, early diagenetic effects such as oxidation on the seafloor can influence the isotopic ratio of organic carbon (see e.g. McArthur *et al.* 1992). Different detrital organic fractions can also be preferentially depleted in carbon during early diagenesis (Benner *et al.* 1987).

This means there are two potential controls on the bulk $\delta^{13}C_{org}$ results described: (1) changes in the isotopic value of dissolved inorganic carbon in the oceans, resulting from increased global carbon burial, and/or (2) changes in organic delivery and preservation.

Palynofacies counts can provide constraint on the organic fractions present in the sample, including the overall proportion of marine vs terrestrial organic matter. In this study, however, AOM was absent on the palynological slides in most samples and yet observed in the un-sieved residues in some samples, meaning it was preferentially lost through the 15 μm mesh used during standard palynological processing (see Section 4.c). Therefore, the palynofacies counts in this study may not be representative of the bulk rock organic content.

5.c.2. Preliminary hypotheses

A PCIE at the DCB and the broad positive trend in $\delta^{13}C_{org}$ through the Kasa Formation are consistent with what is observed globally (see Saltzman, 2002; Saltzman & Thomas, 2012; Kaiser *et al.* 2016), which could suggest it is linked to increased global carbon burial. Considering, though, that the proportion of marine vs terrestrial organic material in bulk rock cannot be quantified (see above) it is premature to link the observed stratigraphic trends and PCIEs in this study solely to global mechanisms. The most positive bulk $\delta^{13}C_{org}$ values are in the uppermost Colpacucho and upper Kasa Formations, both of which are coarser (progradational) units with TOC maxima and higher phytoclast abundance. These results therefore compare well with Davies *et al.* (2012) who observed more positive bulk $\delta^{13}C_{org}$ in coarser sedimentary facies, which was interpreted as reflecting increased terrigenous input.

The characteristics of the organic matter through the 2 ‰ PCIE at the DCB (darker, sparser, more degraded) and the low TOC also suggest that changes in the delivery and preservation of organic matter are a significant controlling factor. It is possible that stress in the terrestrial and marine environments may have caused the reduction in POM (i.e. spores, phytoplankton cyst, plant debris) at the DCB (Fig. 14a–b). This reduction is observed by the sparse POM in the >15 μm palynological fraction and supported by the negative TOC excursion. The remaining POM represents the residual degraded remnants of organic material in the sedimentary system. Assuming a steady flux of AOM, then a reduction in POM delivery would increase the relative proportion of AOM in the samples, resulting in a corresponding shift in bulk $\delta^{13}C_{org}$, i.e. a 2 ‰ PCIE (Fig. 14b). As environmental conditions became less stressed, there was a return of phytoclast- and palynomorph-rich assemblages, resulting in a corresponding $\delta^{13}C_{org}$ negative shift (Fig. 14c). The palynological assemblage above the PCIE is the diminished Tournaisian AI- 2, which shows that EDME occurred coincidentally with these changes in organic matter delivery and preservation. A similar mechanism is possible for the smaller and only partially sampled 1 ‰ PCIE.

The above hypothesis implies that AOM is of a lighter average $\delta^{13}C_{org}$ value than that of POM to cause a positive shift. Carbon fractionation between microbes is highly variable, by as much as 15 ‰ in modern marine phytoplankton (Hinga *et al.* 1994). It would be difficult to infer what types of microbe were responsible for the AOM production based on this study alone. However, a
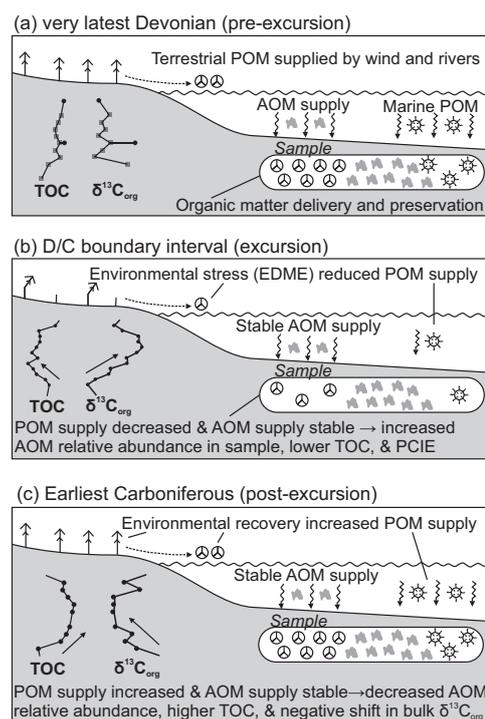

Fig. 14. Interpretation for the 2 ‰ positive carbon isotope excursion at the DCB. (a) Very latest Famennian: pre-excursion. (b) DCB interval excursion. (c) Earliest Tournaisian initial post-excursion.

potential candidate could be green sulphur bacteria, which in one modern species has an average $\delta^{13}C_{org\text{-}cell}$ of −20.2 ‰ (Zyakun *et al.* 2009).

6. Discussion

6.1. Alternative hypothesis of the Cumaná Formation Equivalent Unit

The CFEU is considered part of the Colpacucho Formation by Díaz-Martínez (1992, 1999) and Díaz-Martínez & Isaacson (1994). Based on its sedimentology (i.e. diamictite facies) and similar palynological assemblage (e.g. *Retispora lepidophyta / Umbellasphaeridium* spp.), the unit is considered equivalent to the Cumaná Formation in this study.

Díaz-Martínez (1992) interpreted the diamictites and 22 m overturned beds at Log A road section to be non-glacigenic and the result of debris flows, mass remobilization and the sliding of slabs. Remobilization features complicate any sedimentological interpretation because it is difficult to distinguish between glacial diamictites and debrites from field observations alone (Eyles *et al.* 1985; Visser, 1994). A non-glacigenic interpretation is supported by the absence of exotic clasts and dropstone-in-shale facies in the CFEU, which contrasts with the typical Cumaná Formation (Díaz-Martínez & Isaacson, 1994). Furthermore, debrites are known from the overlying Kasa Formation, which supports a regional stratigraphic interpretation of a progradational clastic wedge on an unstable foreland basin situated NE of an active basin margin (Díaz-Martínez, 1991, 1992, 1996; Sempere, 1995). There are numerous modern and ancient analogues of large-scale mass transport deposits in slope and deep-water settings along active margins (see Alves, 2015); however, this study area would be a unique example of such a system upon a shallow shelf.

A limitation of a purely large-scale remobilization hypothesis is that much of the supporting evidence for sliding slabs and blocks is limited to Log A (Díaz-Martínez, 1992). The CFEU is largely consistent across 7 km and is not observed to be laterally compartmentalized into sliding slabs and/or blocks (Fig. 6a). Also, there is no evidence for shearing or remobilization at the basal incision surface. The 22 m overturned beds at Log A are interpreted by this study to have slipped along a localized décollement surface above a diamictite bed, which would explain its uniqueness in the study area. The sandstone facies, which form the bulk of the topographic ridgeline, are largely depositional in texture, i.e. cross-stratified, laminated or with common ripple mark (Fig. 5a). Deformational features can be present in glacigenic environments, and the range of remobilized features observed are not atypical of an 'ice-traction till' interpretation (see Evans *et al.* 2006). Furthermore, the diamictites can be tracked laterally and have relatively straight contacts and so contrast with the remobilized conglomerates and diamictites in the overlying Kasa Formation, which are small-scale, lobate and/or associated with sheaf folds (see Sections 4.a.3 and 5.a.3).

A glacigenic interpretation is preferred based on the evidence described in this study. However, glacigenic vs remobilized hypotheses should be further tested by sedimentological investigation utilizing microfacies and petrographic analysis. Specifically, the <20 cm striated/grooved gravel beds and overlying diamictites could be sampled for orientated thin-section or magnetic fabric analysis to investigate any textural features indicative of subglacial processes (e.g. van der Meer, 2003). Additional work is also needed to understand the wider palaeogeographic relationship between Colpacucho and Cumaná Formations and the CFEU described in this study.

6.2. The DCB in the western Gondwana

The DCB interval has historically been difficult to identify and correlate in western Gondwana due to the absence/rarity of key fossil groups (conodonts, goniatites, etc.). The findings of this study, if replicated elsewhere in central South America, provide three additional criteria for correlating the DCB interval in western Gondwana and integrating it with the global record of EDME.

Firstly, the boundary lies immediately above diamictite deposits within the lowermost post-glacial sequence. The record of glaciation in the study area is therefore consistent with the wider record of glacial diamictites observed immediately below the DCB within the range of *Retispora lepidophyta* (Caputo *et al.* 2008; Isaacson *et al.* 2008; Lakin *et al.* 2016). Glaciation in the study area is the high-palaeolatitude equivalent of the regressive facies and proxies observed in EDME's lower and middle crisis intervals (Bábek *et al.* 2016; Kaiser *et al.* 2016). The inferred magnitude of incision (<100 m) beneath the CFEU is consistent with the 75–100 m of incision and sea-level fall observed immediately below the DCB in North America (Brezinski *et al.* 2010), Central Europe (van Steenwinkel, 1993) and Moroccan Anti-Atlas (Kaiser *et al.* 2011).

Secondly, the DCB is defined by the sudden loss of *Retispora lepidophyta* and *Umbellasphaeridium saharicum* phytoplankton bioprovince within the initial post-glacial sequence (Vavrdova & Isaacson, 1999). The additional increases in single-walled apiculate miospores and *Gorgonisphaeridium* spp. above the boundary may also provide additional biostratigraphic constraint in western Gondwana where index taxa (e.g. *Vallatisporites vallatus*, *Verrucosisporites nitidus*, *Waltzispora lanzonii*) are rare. These overturns conform with global reference sections where EDME's upper crisis interval is associated with palynological

and marine extinctions during sea-level rise (Streel & Marshall, 2006; Kaiser *et al.* 2016). Furthermore, the early Tournaisian AI-2 in this study is comparable with a contemporaneous diminished palynological record in North America and Europe (Higgs & Streel, 1993; Higgs *et al.*, 1988; Wicander & Playford, 2013).

Thirdly, this study identifies for the first time that the DCB in western Gondwana is coincident with TOC and $\delta^{13}C_{org}$ excursions, comparable to global reference sections (Kaiser *et al.* 2016). The positive $\delta^{13}C_{org}$ excursion observed in this study area starts immediately at the loss of the *R. lepidophyta*, which correlated to the the upper EDME crisis interval and is synchronous with overturns in miospore and phytoplankton assemblages. However, the PCIE observed in this study more likely reflects changes in organic delivery and preservation during an interval of ecological stress rather than being a direct result of global organic carbon drawdown. Further work is needed to test the controls on the 2 ‰ DCB PCIE. This may include processing different maceral types (i.e. phytoclast, phytoplankton, AOM) separately for compound specific biomarkers which would identify the relative proportion of end-member values controlling bulk $\delta^{13}C_{org.}$

6.3. On the cause of palynological extinctions at the DCB

Anoxia has been suggested as a kill mechanism for marine extinctions in the lower EDME crisis interval (Kaiser *et al.* 2016). Paschall *et al.* (2019) identified sustained anoxia into the middle and upper EDME crisis intervals also. In this study, neither obvious 'black shale' facies nor a high TOC value was identified at the DCB, suggesting that marine anoxia was not a factor in the marine phytoplankton extinctions and loss of the *U. saharicum* bioprovince. However, anoxia cannot be discounted, as a low TOC in siliciclastic settings may not preclude anoxic conditions (e.g. Harding *et al.* 2011). Furthermore, even though AOM was qualitatively observed in the whole kerogen samples (i.e. those processed without the 15 μm mesh), there is no constraint on the AOM flux. However, marine anoxia alone cannot explain the coincidence of terrestrial extinctions observed in this study and in the upper crisis interval globally (plants, miospores, placoderms, etc). Due to the observed co-occurrence of marine (phytoplankton) and terrestrial (miospore) extinctions in this study being constrained to the initial post-glacial transgression, rapid climate change associated with the sudden retreat of global ice centres is proposed as the leading cause of extinction in the upper EDME crisis interval. However, additional elemental geochemistry, and Hg/TOC curves in Log E could test marine anoxia and/or magmatic activity as other potential causes of the observed extinctions.

7. Conclusions

The stratigraphy, palynology and chemostratigraphy of a Devonian/Carboniferous boundary section in western Gondwana have been described. A prograding latest Famennian shoreface (Colpacucho Formation) is incised and overlain by a glacigenic unit consisting of coarse sandstones, diamictites and striated/grooved gravel beds (Cumaná Formation Equivalent Unit). The CFEU is at least 7 km wide, 60–120 m thick, and overlies <100 m of incision. Its top surface is a sharp transition into offshore claystones of the lower Kasa Formation, an offshore marine unit recording progradation of regional deltaic systems. The DCB is identified at 12 m above the CFEU on the last occurrence of *Retispora lepidophyta*, with an increase in single-walled apiculate miospores, and loss of the

Umbellasphaeridium saharicum phytoplankton bioprovince. The Tournaisian palynological assemblages are impoverished, and dominated by long-ranging genera with simple morphologies. Coincident with extinction at the DCB is a 2 ‰ positive excursion in bulk $\delta^{13}C_{org}$. This is accompanied by a 0.8 % negative excursion in total organic carbon. It is proposed that environmental stress reduced the supply of particulate organic matter, which increased the relative proportion of amorphous organic matter in the whole-rock samples, thus, causing a shift in average bulk $\delta^{13}C_{org}$. Glaciation in western Gondwana is time-equivalent to eustatic sea-level fall immediately below the DCB. Palynological extinctions occur stratigraphically above diamictites in the initial post-glacial sea-level rise. Terrestrial and marine palynological extinctions observed at the DCB (i.e. the upper EDME crisis interval) are likely related to rapid climate change associated with the sudden retreat of ice centres in western Gondwana and Euramerica.

References

Almond J, Marshall JEA and Evans F (2002) Latest Devonian and earliest Carboniferous glacial events in South Africa. In *Abstract Volume of the 16th IA International Sedimentological Congress, Rand Afrikaans University, Johannesburg, South Africa*, pp. 11–12. Gent: International Association of Sedimentologists.

Alves TM (2015) Submarine slide blocks and associated soft-sediment deformation in deep-water basins: a review. *Marine and Petroleum Geology* **67**, 262–85. doi:10.1016/j.marpetgeo.2015.05.010.

Aretz M, Herbig HG and Wang XD (2016) The Carboniferous Period. In *The Geological Time Scale 2020* (eds FM Gradstein, JG Ogg, MD Schmitz and GM Ogg), pp. 811–74. Amsterdam: Elsevier.

Bábek O, Kumpan T, Kalvoda J and Grygar TM (2016) Devonian/ Carboniferous boundary glacioeustatic fluctuations in a platform-to-basin direction: a geochemical approach of sequence stratigraphy in pelagic settings. Sedimentary Geology 337, 81–99. doi: 10.1016/j.sedgeo.2016.03.009.

Barnes JB, Ehler TA, Insei N, McQuarrie N and Poulson CJ (2012) Linking orography, climate, and exhumation across the central Andes. *Geology* **40**, 1135–8. doi: 10.1130/G33229.1.

Becker RT (1992) Analysis of ammonoid palaeobiogeography in relation to the global Hangenberg (terminal Devonian) and Lower Alum Shale (Middle Tournaisian) events. *Annales de la Société Géologique de Belgique* **115**, 459–73.

Becker RT, Kaiser SI and Aretz M (2016) Review of chrono-, litho- and biostratigraphy across the global Hangenberg Crisis and Devonian-Carboniferous Boundary. In *Devonian Climate, Sea Level and Evolutionary Events* (eds RT Becker, P Königshof and CE Brett), pp. 355–86. Geological Society of London, Special Publication no. 423. doi: 10.1144/SP423.10.

Becker RT, Marshall JEA and Da Silva A-C (2020) The Devonian Period. In *The Geological Time Scale 2020* (eds FM Gradstein, JG Ogg, MD Schmitz and GM Ogg), pp. 733–810. Amsterdam: Elsevier.

Benner R, Fogel ML, Sprague EK and Hodson RE (1987) Depletion of ^{13}C in lignin and its implications for stable isotope studies. *Nature* **329**, 708–10. doi: 10.1038/329708a0.

Brand U, Legrand-Blain M and Street M (2004) Biochemostratigraphy of the Devonian- Carboniferous boundary global stratotype section and point, Griotte Formation, La Serre, Montagne Noire, France. *Palaeogeography,*

Palaeoclimatology, Palaeoecology **205**, 337–57. doi: 10.1016/j.palaeo.2003. 12.015.

Brezinski DK, Blaine-Cecil C and Skema VW (2010) Late Devonian glacigenic and associated facies from the central Appalachian Basin, eastern United States. *GSA Bulletin* **122**, 265–81. doi: 10.1130/B26556.1.

Brezinski DK, Cecil CB, Skema VW and Stamm R (2008) Late Devonian glacial deposits from the eastern United States signal an end of the mid-Paleozoic warm period. *Palaeogeography, Palaeoclimatology, Palaeoecology* **268**, 143–51. doi: 10.1016/j.palaeo.2008.03.042.

Buggisch W and Joachimski MM (2006) Carbon isotope stratigraphy of the Devonian of Central and Southern Europe. *Palaeogeography, Palaeoclimatology, Palaeoecology* **240**, 68–88.

Capitano FA, Faccenna C, Zlotnik S and Stegman DR (2011) Subduction dynamics and the origin of Andean orogeny and the Bolivian orocline. *Nature* **480**, 83–6. doi: 10.1038/nature10596.

Caputo MV and Dos Santos ROB (2019) Stratigraphy and ages of four Early Silurian through Late Devonian, Early and Middle Mississippian glaciation events in the Parnaíba Basin and adjacent areas, NE Brazil. *Earth-Science Reviews* **207**, 103002. doi: 10.1016/j.earscirev.2019.103002.

Caputo MV, Melo JHG, Street M and Isbell JL (2008) Late Devonian and Early Carboniferous glacial records of South America. In *Resolving the Late Paleozoic Ice Age in Time and Space* (eds CR Fielding, TD Frank and JL Isbell), pp. 161–73. Boulder, Colorado: Geological Society of America Special Paper no. 441.

Carling PA (1990) Particle over-passing on depth-limited gravel bars. *Sedimentology* **37**, 345–55.

Carmichael SK, Waters JA, Batchelor CJ, Coleman DM, Suttner TJ, Kido E, Moore LM and Chadimová L (2016) Climate instability and tipping points in the Late Devonian: detection of the Hangenberg Event in an open oceanic island arc in the Central Asian Orogenic Belt. *Gondwana Research* **32**, 213–31. doi: 10.1016/j.gr.2015.02.009.

Chlupáč I, Feist R and Morzadec P (2000) Trilobites and standard Devonian stage boundaries. *Courier Forschungsinstitut Senckenberg* **220**, 87–98.

Clayton G, Coquel R, Doubinger J, Gueinn KJ, Loboziak S, Owens B and Streel M (1977) Carboniferous miospores from Western Europe: illustrations and zonation. *Mededelingen Rijks Geologische Dienst* **29**, 1–71.

Corradini C, Spalletti C, Kaiser SI and Matyja H (2013) Overview of conodonts across the Devonian/Carboniferous boundary. In *Conodonts from the Andes: Proceedings of the 3rd International Conodont Symposium & Regional Field Meeting of the IGCP Project 591* (eds GL Albanesi and G Ortega), pp. 13–16. Buenos Aires: Asociación Paleontológica Argentina, Publicación Especial.

Cramer BD, Saltzman MR, Day JE and Witzke J (2008) Record of the Late Devonian Hangenberg global positive carbon-isotope excursion in an epeiric sea setting: carbonate production, organic-carbon burial and paledaooceanograhy during the Late Famennian. In *Dynamics of Epeiric Seas* (eds B Pratt and C Holmden), pp. 103–18. Saint John's: Geological Association of Canada Special Paper no. 48.

Cunha PRC, Melo JHG and Silva OB (2007) Bacia do Amazonas. *Boletim de Geociências da Petrobras* **15**, 227–51.

Daemon RF (1974) Palinomorfos-guias do Devoniano Superior e Carbonífero Inferior das bacias do Amazonas e Parnaíba. *Anais da Academia Brasileira de Ciências* **46**, 549–87.

Davies SJ, Leng MJ, MacQuaker JHS and Hawkins K (2012) Sedimentary process control on carbon isotope composition of sedimentary organic matter in an ancient shallow-water shelf succession. *Geochemistry, Geophysics, Geosystems* **13**, 1–15. doi: 10.1029/2012004218.

Di Pasquo M, Grader G, Isaacson PE, Souza PA, Iannuzzi R and Díaz-Martínez E (2015) Global biostratigraphic comparison and correlation of an early Cisuralian palynoflora from Bolivia. *Historical Biology* **27**, 1–30. doi: 10.1080/08912963.2014.910204.

Díaz-Martínez E (1991) Litoestratigrafia del Carbonífero del Altiplano de Bolivia. *Revista Tecnica de YPFB* **12**, 295–302.

Díaz-Martínez E (1992) Inestabilidad tectónica en el Devónico superior del Altiplano de Bolivia: evidencias en el registro sedimentario. In *Actas del III Congreso Geológico de España y VIII Congreso Latino-americano de Geología*, University of Salamanca, pp. 35–9.

Díaz-Martínez E (1993) The Carboniferous sequence of the northern Altiplano of Bolivia: from glacial-marine to carbonate deposition. *Comptes Rendus XII ICC-P* **2**, 203–22.

Díaz-Martínez E (1996) Sintesis estratigrafica y geodynamica del Carbonifero de Bolivia. *Memorias del XII Congreso Geologico de Bolivia*, 355–67.

Díaz-Martínez E and Isaacson PE (1994) Late Devonian glacially-influenced marine sedimentation in western Gondwana: the Cumana Formation, Altiplano, Bolivia. In *Pangea: Global Environments and Resources* (eds AF Embry, B Beauchamp and DJ Glass), pp. 511–22. Calgary: Canadian Society of Petroleum Geologists Memoir no. 17.

Díaz-Martínez E, Vavrdová M, Bek J and Isaacson PE (1999) Late Devonian (Famennian) glaciation in Western Gondwana: evidence from the Central Andes. *Abhandlungen der Geologischen Bundesanstalt* **54**, 213–37.

Domeier M and Torsvik TH (2014) Plate tectonics in the late Paleozoic. *Geoscience Frontiers* **5**, 303–50.

Ettensohn FR, Lierman RT and Mason CE (2009) Upper Devonian–Lower Mississippian clastic rocks in northeastern Kentucky: evidence for Acadian alpine glaciation and models for source-rock and reservoir rock development in the eastern United States. American Institute of Professional Geologists – Kentucky Section Spring Field Trip, 18 April 2009. 1–63.

Evans DJA, Phillips ER, Hiemstra JF and Auton CA (2006) Subglacial till: formation, sedimentary characteristics and classification. *Earth Science Reviews* **78**, 115–76.

Evans FJ (1999) Paleobiology of Early Carboniferous lacustrine biota of the Waaipoort Formation (Witteberg Group), South Africa. *Palaeontologia Africana* **35**, 1–6.

Eyles C, Eyles N and Miall AD (1985) Models of glaciomarine sedimentation and their application to the interpretation of ancient glacial sequences. *Palaeogeography, Palaeoclimatology, Palaeoecology* **51**, 15–84. doi: 10.1016/0031-0182(85)90080-X.

Filho JRW, Eiras JF and Vaz PT (2007) Bacia do Solimoes. *Boletim de Geociencias da Petrobras* **15**, 217–25.

Flint RF, Sanders JE and Rodgers J (1960a) Symmictite: a name for nonsorted terrigenous sedimentary rocks that contain a wide range of particle sizes. *Geological Society of America Bulletin* **71**, 507–10.

Flint RF, Sanders JE and Rodgers J (1960b) Diamictite, a substitute term for symmictite. *Geological Society of America Bulletin* **71**, 1809–10.

Grader G, Díaz-Martínez E, Davydov V, Montanez I, Tair J and Isaacson PE (2007) Late Paleozoic stratigraphic framework in Bolivia: constraints from the warm water Cuevo megasequence. *4th European Meeting on the Palaeontology and Stratigraphy of Latin America* (eds E Díaz-Martínez and EL Rabano), pp. 181–7. Instituto Geologico y Minera de Espana, Cuadernos del Museo Geominero, no. 8, Madrid. https://www.worldcat.org/title/4th-european-meeting-on-the-palaeontology-and-stratigraphy-of-latin-america-tres-cantos-madrid-september-12-14-2007/oclc/820824344.

Gregory-Wodzicki K M (2000) Uplift history of the Central and Northern Andes: a review. *GSA Bulletin* **112**, 1091–1105.

Harding IC, Charles AJ, Marshall JEA, Pälike H, Roberts AP, Wilson PA, Jarvis E, Thorne R, Morris E, Moreman R, Pearce RB and Akbari S (2011) Sea-level and salinity fluctuations during the Paleocene-Eocene thermal maximum in Arctic Spitsbergen. *Earth and Planetary Science Letters* **303**, 97–107.

Herbig H-G, Korn D, Amler MRW, Hartenfels S and Jäger H (2019) The Mississippian Kulm Basin of the Rhenish Mountains, western Germany: fauna, facies, and stratigraphy of a mixed carbonate-siliciclastic foreland basin. *Kölner Forum für Geologie und Paläontologie* **24**, 143–217.

Higgs KT, Clayton G and Keegan JB (1988) Stratigraphy and systematic palynology of the Tournaisian rocks of Ireland. *The Geological Survey of Ireland Special Paper* **7**, 93 pp.

Higgs KT and Streel M (1993) Palynological age for the lower part of the Hangenberg Shales in Sauerland, Germany. *Annales de la Société Géologique de Belgique* **116**, 243–7.

Hinga KR, Arthur MA, Pilson MEQ and Whitaker D (1994) Carbon fractionation by marine phytoplankton in culture: the effects of CO_2 concentration, pH, and species. *Global Biogeochemical Cycles* **8**, 91–102.

Hornung JJ, Asprion U and Winsemann J (2007) Jet-efflux deposits of a subaqueous ice contact fan, glacial Lake Rinteln, northwestern Germany. *Sedimentary Geology* **193**, 167–92. doi: 10.1016/j.sedgeo.2005.11.024.

Isaacson P, Díaz-Martínez E, Grader G, Kaldova J, Bábek O and Devuyst FX (2008) Late Devonian–earliest Mississippian glaciation in Gondwanaland and its biogeographic consequences. *Palaeogeography, Palaeoclimatology, Palaeoecology* **268**, 126–42. doi: 10.1016/j.palaeo.2008.03.047.

Isaacson PE, Palmer BA, Mamet BL, Cooke JC and Sanders DE (1995) Devonian-Carboniferous stratigraphy in the Madre de Dios Basin, Bolivia: Pando X-1 and Manuripi X-1 wells. In Petroleum Basins of South America (eds AJ Tankard, R Suarez and HJ Welsink), pp. 501–511. American Association of Petroleum Geologists Memoirs, v. 62.

Jardiné S, Combaz A, Magloire L, Peniguel G and Vachey G (1974) Distribution stratigraphique des acritarches dans le Paleozoïque du Sahara Algérien. *Review of Palaeobotany and Palynology* **18**, 99–129. doi: 10.1016/0034-6667(74)90012-8.

Kaiser SI, Aretz M and Becker RT (2016) The global Hangenberg Crisis (Devonian – Carboniferous transition): review of a first-order mass extinction. In *Devonian Climate, Sea Level and Evolutionary Events* (eds RT Becker, P Königshof and CE Brett), pp. 387–437. Geological Society of London, Special Publication no. 423. doi: 10.1144/SP423.9.

Kaiser SI, Becker RT, Hartenfels S and Aboussalem ZS (2013) Middle Famennian to middle Tournaisian stratigraphy at El Atrous (Amessoui syncline, southern Tafilalt). In *International Field Symposium 'The Devonian and Lower Carboniferous of northern Gondwana'* (eds RT Becker, A El Hassani and A Abdelfatah), pp. 77–87. Document de l'Institut Scientifique, Rabat, no. 27.

Kaiser SI, Becker RT, Steuber T and Aboussalem ZS (2011) Climate controlled mass extinctions, facies, and sea-level changes around the Devonian-Carboniferous boundary in the eastern Anti-Atlas (SE Morocco). *Palaeogeography, Palaeoclimatology, Palaeoecology*, **310**, 340–64. doi: 10.1016/j.palaeo.2011.07.026.

Kaiser SI, Steuber T and Becker RT (2008) Environmental change during the Late Famennian and Early Tournasian (Late Devonian-Early Carboniferous): implications from stable isotopes and conodont biofacies in Southern Europe. *Geological Journal* **43**, 241–60. doi: 10.1002/gj.1111.

Klett TR (2000) Total Petroleum Systems of the Trias/Ghadames Province, Algeria, Tunisia, and Libya –The Tanezzuft–Oued Mya, Tanezzuft–Melrhir, and Tanezzuft–Ghadames. United States Geological Survey, Bulletin, 2202-C. doi: 10.3133b2202C.

Komatsu T, Kato S, Hirata K, Takashima R, Ogata Y, Oba M, Naruse H, Ta PH, Nguyen PD, Dang HT, Doan TN, Nguyen HH, Sakata S, Kaiho K and Konigshof P (2014) Devonian-Carboniferous transition containing a Hangenberg Black Shale equivalent in the Pho Han Formation on Cat Ba Island, northeastern Vietnam. *Palaeogeography, Palaeoclimatology, Palaeoecology* **404**, 30–43. doi: 10.1016/j.palaeo.2014.03.021.

Könitzer SF, Davies SJ, Stephenson MH and Leng MJ (2014) Depositional controls on mudstone lithofacies in a basinal setting: implications for the delivery of sedimentary organic matter. *Journal of Sedimentary Research* **84**, 198–214. doi: 10.2110/jsr.2014.18.

Kumpan T, Bábek O, Kalvoda J, Frýda J and Grygar T M (2013) A high-resolution, multiproxy stratigraphic analysis of the Devonian–Carboniferous boundary sections in the Moravian Karst (Czech Republic) and a correlation with the Carnic Alps (Austria). *Geological Magazine* **151**, 201–15. doi: 10.1017/S0016756812001057.

Kumpan T, Bábek O, Kalvoda J, Grygar TM and Frýda J (2014) Sea-level and environmental changes around the Devonian–Carboniferous boundary in the Namur–Dinant Basin (S Belgium, NE France): a multi-proxy stratigraphic analysis of carbonate ramp archives and its use in regional and inter-regional correlations. Sedimentary Geology 311, 43–59. doi: 10.1016/j.sedgeo.2014.06.007.

doidoi:**Lakin JA, Marshall JEA, Troth I and Harding IC** (2016) Greenhouse to icehouse: a biostratigraphic review of latest Devonian–Mississippian glaciations and their global effects. In *Devonian Climate, Sea Level and Evolutionary Events* (eds RT Becker, P Königshof and CE Brett), pp. 423–39. Geological Society of London, Special Publication no. 423. doi: 10.1144/SP423.12.

Le Heron DP, Sutcliffe OE, Whittington RJ and Craig J (2005) The origins of glacially related soft-sediment deformation structures in Upper Ordovician glaciogenic rocks: implication for ice-sheet dynamics. *Palaeogeography, Palaeoclimatology, Palaeoecology* **218**, 75–103. doi: 10.1016/j.palaeo.2004.12.007.

Liu F, Kerp H, Peng H and Zhu H (2019) Palynostratigraphy of the Devonian–Carboniferous transition in the Tulong section in South Tibet: a Hangenberg Event sequence analogue in the Himalaya-Tethys zone. *Palaeogeography, Palaeoclimatology, Palaeoecology* **531**. doi: 10.1016/j.palaeo.2018.03.016.

Loboziak S, Caputo MV and Melo JHG (2000) Middle Devonian-Tournaisian miospore biostratigraphy in the southwestern outcrop belt of the Parnaiba basin, north-central Brazil. *Revue de Micropaleontologie* **43**, 301–18. doi: doi: 10.1016/S0035-1598(00)90154-5.

Loboziak S, Caputo MV and Owens B (1986) *Aratrisporites saharaensis* sp. nov. A characteristic Lower Carboniferous miospore species of North Africa. *Geobios* **19**, 497–503.

Loboziak S and Melo JHG (2002) Devonian miospore successions of Western Gondwana: update and correlation with Southern Euramerican miospore zones. *Review of Palaeobotany and Palynology* **121**, 133–48. doi: doi: 10.1016/S0034-6667(01)00098-7.

Loboziak S, Melo JHG, Playford G and Streel M (1999) The *Indotriradites dolianitii* Morphon, a distinctive group of miospore species from the Lower Carboniferous of Gondwana. *Review of Palaeobotany and Palynology* **107**, 17–22. doi: 10.1016/S0034-6667(99)00016-0.

Loboziak S, Melo JHG and Streel M (2005) Devonian palynostratigraphy in western Gondwana. In *Applied Stratigraphy* (ed. EAM Koutsoukos), pp. 73–99. Dordrecht: Springer.

Marshall JEA (2020) A terrestrial Devonian-Carboniferous boundary section in East Greenland. *Palaeobiodiversity and Palaeoenvironments*. doi: 10.1007/s12549-020-00448-x.

Matyja H, Woroncowa-Marcinowska T, Filipiak P, Brański P and Sobień K (2020) The Devonian/Carboniferous boundary interval in Poland: multidisciplinary studies in pelagic (Holy Cross Mountains and Sudetes) and ramp (Western Pomerania) successions. *Palaeobiodiversity and Palaeoenvironments* **101**, 421–72. doi: 10.1007/s12549-020-00442-3.

Maziane N, Higgs KT and Streel M (1999) Revision of the late Famennian miospore zonation scheme in eastern Belgium. *Journal of Micropalaeontology* **18**, 17–25.

Maziane N, Higgs KT and Streel M (2002) Biometry and paleoenvironment of *Retispora lepidophyta* (Kedo) Playford 1976 and associated miospores in the latest Famennian nearshore marine facies, eastern Ardenne (Belgium). *Review of Palaeobotany and Palynology* **118**, 211–26.

McArthur JM, Tyson RV, and Mattey D (1992) Early diagenesis of marine organic matter: alteration of the carbon isotopic composition. *Marine Geology* **105**, 51–61. doi: 10.1016/0025-3227(92)90181-G.

Melo JHG and Loboziak S (2000) Visean miospore biostratigraphy and correlation of the Poti Formation (Parnaíba Basin, northern Brazil). *Review of Palaeobotany and Palynology* **112**, 147–65. doi: 10.1016/S0034-6667(00)00043-9.

Melo JHG and Loboziak S (2003) Devonian/Early Carboniferous miospore biostratigraphy of the Amazon Basin, Northern Brazil. *Review of Palaeobotany and Palynology* **124**, 131–202. doi: 10.1016/S0034-6667(02)00184-7.

Melo JHG and Playford G (2012) Miospore palynology and biostratigraphy of Mississippian strata of the Amazona Basin, northern Brazil. Part Two. *AASP Contribution Series* **47**, 93–201.

Middleton GV (2003) Tool marks. In *Encyclopedia of Sediments and Sedimentary Rocks* (eds GV Middleton, MC Church, M Coniglio, LA Hardie and FJ Longstaffe), pp. 747–8. Dordrecht: Springer. doi:10.1007/978-1-4020-3609-5_240.

Milani EJ, Melo JHG, Souza PA, Fernandez LA and Franca AB (2007) Bacia do Parana. *Boletime Geociencias da Petrobras* **15**, 265–287.

Moncrieff ACM (1989) Classification of poorly-sorted sedimentary rocks. *Sedimentary Geology* **65**, 191–4. doi: doi: 10.1016/0037-0738(89)90015-8.

Myrow P (2003) Gutters and gutter casts. In *Encyclopedia of Sediments and Sedimentary Rocks* (eds GV Middleton, MC Church, M Coniglio, LA Hardie and FJ Longstaffe), Dordrecht: Springer. doi:10.1007/978-1-4020-3609-5_107.

Myrow PM, Hanson A, Phelps AS, Creveling JR, Strauss JV, Fike DA and Ripperdan RL (2013) Latest Devonian (Famennian) global events in western Laurentia: variations in the carbon isotopic record linked to diagenetic alteration below regionally extensive unconformities. *Palaeogeography,*

Palaeoclimatology, Palaeoecology **386**, 194–209. doi: 10.1016/j.palaeo.2013.05.021.

Myrow PM, Strauss H, Creveling JR, Sicard KR, Ripperdan R, Sandberg CA and Hartenfels S (2011) A carbon isotopic and sedimentological record of the latest Devonian (Famennian) from the Western U.S. and Germany. *Palaeogeography, Palaeoclimatology, Palaeoecology* **306**, 147–59.

Over DJ (2020) The Devonian-Carboniferous boundary in the United States. *Palaeobiodiversity and Palaeoenvironments*. doi: 10.1007/s12549-020-00428-1.

Pacton M, Gorin GE and Vasconcelos C (2011) Amorphous organic matter: experimental data on formation and the role of microbes. *Review of Palaeobotany and Palynology* **166**, 253–67.

Paschall O, Carmichael SK, Königshof P, Waters JA, Ta PH, Komatsu T and Dombrowski A (2019) The Devonian-Carboniferous boundary in Vietnam: sustained ocean anoxia with a volcanic trigger for the Hangenberg Crisis? *Global and Planetary Change* **175**, 64–81. doi 10.1016/j.gloplacha.2019.01.021.

Phipps D and Playford G (1984) Laboratory techniques for extraction of palynomorphs from sediments. *Papers, Department of Geology, University of Queensland* **11**, 1–23.

Piotrowski JA, Geletneky J and Vater R (1999) Soft-bedded subglacial melt-water channel from the Welzow-Sud opencast lignite mine, Lower Lusatia, eastern Germany. *Boreas* **28**, 363–74.

Piotrowski JA, Mickelson DM, Tulaczyk S, Krzyszowski D and Junge FW (2001) Were deforming beds beneath past ice sheets really widespread? *Quaternary International* **97–98**, 173–7.

Pisarzowska A and Racki G (2020) Comparative carbon isotope chemostratigraphy of major Late Devonian biotic crises. In *Stratigraphy and Timescales, vol. 5* (ed. M Montenari), pp. 387–466. Amsterdam: Elsevier.

Pisarzowska A, Rakociński M, Marynowski L, Szczerba M, Thoby M, Paszkowski M, Perri MC, Spalletta C, Schönlaub H-P, Kowalik N and Gereke M (2020) Large environmental disturbances caused by magmatic activity during the Late Devonian Hangenberg Crisis. *Global and Planetary Change* **190**. doi:10.1016/j.gloplacha.2020.103155.

Playford G and Melo JHG (2009) The Mississippian miospore *Neoraistrickia loganensis* (Winslow, 1962) Coleman and Clayton, 1987: morphological variation and stratigraphic and palaeogeographic distribution. *Revista Española de Micropaleontología* **41**, 241–54.

Playford G and Melo JHG (2010) Morphological variation and distribution of the Tournaisian (Early Mississippian) miospore *Waltzispora lanzonii* Daemon 1974. *Neues Jahrbuch für Geologie und Paläontologie Abhandlungen* **256**, 183–93. doi: 10.1127/0077-7749/2010/0 043.

Playford G and Melo JHG (2012) Miospore palynology and biostratigraphy of Mississippian strata of the Amazonas Basin, northern Brazil. Part One. *AASP Contribution Series* **47**, 3–89.

Prestianni C, Sautois M and Denayer J (2016) Disrupted continental environments around the Devonian Carboniferous Boundary: introduction of the tener event. *Geologica Belgica* **19**, 135–45.

Qie W, Liu J, Chen J, Wang X, Mii H -S, Zhang X, Huang X, Yao L, Algeo TJ and Luo G (2015) Local overprints on the global carbonate δ13C signal in Devonian– Carboniferous boundary successions of South China. *Palaeogeography, Palaeoclimatology, Palaeoecology* **418**, 290–303. doi: 10.1016/j.palaeo.2014.11.022.

Sallan LC and Coates MI (2010) End-Devonian extinction and a bottleneck in the early evolution of modern jawed vertebrates. *PNAS*, **107**, 10131–5. doi: 10.1073/pnas.0914000107.

Saltzman MR (2002) Carbon and oxygen isotope stratigraphy of the Lower Mississippian (Kinderhookian–lower Osagean), western United States: implications for seawater chemistry and glaciation. *GSA Bulletin* **114**, 96–108.

Saltzman MR (2005) Phosphorus, nitrogen, and the redox evolution of the Paleozoic oceans. *Geology* **33**, 573–6. doi: 10.1130/G21535.1.

Saltzman MR and Thomas E (2012) Carbon isotope stratigraphy. In *The Geological Time Scale 2012* (eds FM Gradstein, JG Ogg, MD Schmitz and GM Ogg), pp. 207–38. Amsterdam: Elsevier.

Sarjeant WAS and Stancliffe RPW (1994) The *Michrystridium* and *Veryhachium* complexes (Acritarcha: Acanthomorphitae and Polygonomorphitae): a taxonomic reconsideration. *Micropaleontology* **40**, 1–77.

Sempere T (1995) Phanerozoic evolution of Bolivia and adjacent regions. In *Petroleum Basins of South America* (eds AJ Tankard, R Suarez and HJ Welsink), pp. 207–30. AAPG Memoirs no. 57.

Servais T, Vecoli M, Li J, Molyneux SG, Raevskaya EG and Rubinstein CV (2007) The Acritarch Genus *Veryhachium* Deunff 1954: taxonomic evaluation and first appearance. *Palynology* 31, 191–203. doi: 10.2113/gspalynol.31.1.191.

Streel M, Caputo MV, Loboziak S, Melo JHG and Thorez J (2000) Palynology and sedimentology of laminites and tillites from the latest Famennian of the Parnaiba basin, Brazil. *Geologica Belgica* 3, 87–96.

Streel M, Higgs KT, Loboziak S, Riegal W and Steemans P (1987) Spore stratigraphy and correlation with faunas and floras in the type marine Devonian of the Ardenne-Rhenish regions. *Review of Palaeobotany and Palynology* 50, 211–29. doi: 10.1016/0034-6667(87)90001-7.

Streel M and Marshall JEA (2006) Devonian–Carboniferous boundary global correlations and their paleogeographic implications for the assembly of Pangaea. In *Proceedings of the XVth International Congress on Carboniferous and Permian Stratigraphy* (ed. TE Wong), pp. 481–96. Amsterdam: Royal Netherlands Academy of Arts and Sciences, 2007. https://www.worldcat.org/title/proceedings-of-the-xvth-international-congress-on-carboniferous-and-permian-stratigraphy/oclc/85777910.

Streel M and Theron JN (1999) The Devonian-Carboniferous boundary in South Africa and the age of the earliest episode of the Dwyka glaciation: new palynological result. *Episodes* 22, 41–4.

Talling PJ, Masson DG, Sumner EJ and Malgesini G (2012) Subaqueous sediment density flows: depositional processes and deposit types. *Sedimentology* 59, 1937–2003.

Theron JH (1993) The Devonian–Carboniferous boundary in South Africa. *Annales de la Societe Geologique de Belgique* 116, 291–300.

Troth I, Marshall JEA, Racey A and Becker T (2011) Devonian sea-level change in Bolivia: a high palaeolatitude biostratigraphical calibration of the global sea-level curve. *Palaeogeography, Palaeoclimatology, Palaeoecology* 304, 3–20. doi: 10.1016/j.palaeo.2010.10.008.

Van der Meer JJM (2003) Subglacial till: the deforming glacier bed. *Quaternary Science Reviews* 22, 1659–85. doi: 10.1016/S0277-3791(03)00141-0.

Van Steenwinkel M (1993) The Devonian–Carboniferous boundary: comparison between the Dinant synclinorium and the northern border of the Rhenish Slate Mountains, a sequence-stratigraphic view. *Annales de la Société Géologique de Belgique* 115, 665–81.

Vavrdová M and Isaacson PE (1999) Late Famennian phytogeographic provincialism: evidence for a limited separation of Gondwana and Laurentia. *Abhandlungen der Geologischen Bundesanstalt* 54, 453–63.

Vaz PT, Mata Rezende NGA, Filho JRW and Travassos WAS (2007) Bacia do Parnaíba. *Boletim de Geociências da Petrobras* 15, 253–63.

Vesely FF and Assine ML (2014) Ice-keel scour marks in the geological record: evidence from Carboniferous soft-sediment striated surfaces in the Parana Basin, Southern Brazil. *Journal of Sedimentary Research* 84, 26–39. doi: 10.2110/jsr.2014.4.

Visser JNJ (1994) The interpretation of massive rain-out and debris-flow diamictites from the glacial marine environment. In *Earth's Glacial Record* (eds M Deynoux, JMG Miller, EW Domack, N Eyles, IJ Fairchild and GM Young), pp. 83–93.

Weber LJ, Francis BP, Harris PM and Clarke M (2008) Stratigraphy, lithofacies and reservoir distribution – Tengiz Field, Kazakhstan. *Search and Discovery Article* #20059, 1–4.

Wicander R, Clayton G, Marshall JEA, Troth I and Racey A (2011) Was the latest Devonian glaciation a multiple event? New palynological evidence from Bolivia. *Palaeogeography, Palaeoclimatology, Palaeoecology* 305, 75–83. doi: 10.1016/j.palaeo.2011.02.016.

Wicander R and Playford G (2013) Marine and terrestrial palynofloras from transitional Devonian-Mississippian strata, Illinois Basin, U.S.A. *Boletin Geologico y Minero* 124, 589–637.

Woodforth-Lynas C and Dowdeswell JA (1994) Soft-sediment striated surfaces and massive diamicton facies produced by floating ice. In *Earth's Glacial Record* (eds M Deynoux, JMG Miller, EW Domack, N Eyles, IJ Fairchild and GM Young), pp. 241–59.

Zyakun AM, Lunina ON, Prusakova TS, Pimenov NV and Ivanov MV (2009) Fractionation of stable carbon isotopes by photoautotrophically growing anoxygenic purple and green sulfur bacteria. *Microbiology* 78, 757–68.